Final Report
on
ISTC Contract # 1809p

Parametric Study of Advanced Mixing of Fuel/Oxidant System in High Speed Gaseous Flows and Experimental Validation Planning. (comprehensive)

Prepared for EOARD

Project Manager

Valentin A. BITYURIN, PhD, DS

Dr.A.N.Bocharov
Dr.D.S.Baranov

Moscow
August 30, 2001

REPORT DOCUMENTATION PAGE

Form Approved OMB No. 0704-0188

PLEASE DO NOT RETURN YOUR FORM TO THE ABOVE ADDRESS.

1. REPORT DATE *(DD-MM-YYYY)*	2. REPORT TYPE	3. DATES COVERED *(From – To)*
28-10-2001	Final Report	01-Jun-00 - 01-Jun-01

4. TITLE AND SUBTITLE

Parametric Study of Advanced Mixing of Fuel/Oxidant System in High Speed Gaseous Flows and Experimental Validation Planning

5a. CONTRACT NUMBER
ISTC Registration No: 1809

5b. GRANT NUMBER

5c. PROGRAM ELEMENT NUMBER

6. AUTHOR(S)

Dr. Valentin Bityurin

5d. PROJECT NUMBER

5d. TASK NUMBER

5e. WORK UNIT NUMBER

7. PERFORMING ORGANIZATION NAME(S) AND ADDRESS(ES)

Institute of High Temperatures RAS (IVTAN)
Izhorskaya str., 13/19
Moscow 127412
Russia

8. PERFORMING ORGANIZATION REPORT NUMBER

N/A

9. SPONSORING/MONITORING AGENCY NAME(S) AND ADDRESS(ES)

EOARD
PSC 802 BOX 14
FPO 09499-0014

10. SPONSOR/MONITOR'S ACRONYM(S)

11. SPONSOR/MONITOR'S REPORT NUMBER(S)
ISTC 00-7008

12. DISTRIBUTION/AVAILABILITY STATEMENT

Approved for public release; distribution is unlimited.

13. SUPPLEMENTARY NOTES

14. ABSTRACT

This report results from a contract tasking Institute of High Temperatures RAS (IVTAN) as follows: One of the main problems of stable combustion in high-speed flow is an effective mixing of gaseous fuel and oxidant providing full combustion during the resident time in combustor chamber. Generally speaking in-flow mixing consists of two main mechanisms: kinematics mixing (convection) and molecular diffusion. The latter is a final stage of mixing needed to provide extended combustible mixture. Kinematics mixing is more effective in vortex flows; the higher vorticity the better kinematics mixing which means the larger fuel/oxidant interface surface. The second mixing mechanisms – diffusion forms a reacting volume estimated as the interface surface times diffusion length. Both interface surface and diffusion length are increasing functions of time. Having these two functions explicitly one can calculate a reacting volume formation and, with chemical kinetics scheme known, the combustion process can be described in detailed. Such an approach has been developed in IVTAN for simulation of high-speed flow of chemically reacting mixture for plasma chemistry applications and simulation of combustion in compressor-type chemical reactors basing on Diesel engine.

Because of very short residence time is typical of ram/scram jet operation conditions the measures providing a significant increasing rate of reacting volume are very actual.

The proposed Advanced Mixing approach is to increase the reacting volume growth by (1) pulse electrical discharge - JE energy release and (2) by MHD interaction - J?B body force.

Furthermore it was found recently both experimentally and theoretically [1] that under certain conditions typical of so called Plasma Aerodynamics experiments the filamentary structure of high frequency discharge (streamer discharge) results some times in high speed counterflow jet formation. Such a jet can transfer a significant mass of fluid from one point to another rather distant location. Thus, providing a controllable filamentary discharge across a primary fuel/oxidant interface one can intensify the initial mixing of fuel/oxidant composition.

The second component of Advanced Mixing is vortex generation by a highly non-potential J?B body force. This force is defined by current density component J? perpendicular to the external applied magnetic field B.

The preliminary information about such a mixing process was collected in IVTAN while an MHD generator flow with current-currying non-uniformities was studied. At that time the main question was how to decrease the mixing process intensified by vorticity generation. Now the amplification of mixing by MHD and Pulse Plasma affects should be studied in turn and recommended.

We have developed earlier (see, for example [2,3] and others publications) physical and numerical models to treat the kinematic and diffusion mixing in gas-plasma flows to evaluate the life time of plasmoids in such a flow under intensive MHD interaction conditions.

It is proposed now at first to adopt these approaches to the physically similar situation of mixing of gaseous fuel and oxidant.

The second goal of the project is to use the models developed under the first task to conduct parametric study of effects of Advanced Mixing on characteristics of fuel/oxidant mixing in high speed flows.

The third goal is the project is to formulate preliminary the scheme of the experimental validation of proposed approach under experimental conditions available at IHT RAS.

15. SUBJECT TERMS
EOARD, Propulsion, Engines and Fuels, Combustion & Ignition

16. SECURITY CLASSIFICATION OF:			**17. LIMITATION OF ABSTRACT**	**18, NUMBER OF PAGES**	**19a. NAME OF RESPONSIBLE PERSON**
a. REPORT	**b. ABSTRACT**	**c. THIS PAGE**			Charbel N. Raffoul
UNCLAS	UNCLAS	UNCLAS	UL	57	**19b. TELEPHONE NUMBER** *(Include area code)* +44 (0)20 7514 4299

Standard Form 298 (Rev. 8/98)
Prescribed by ANSI Std. Z39-18

This report is the final report as it indicated in the Supplement 2 to the Work Plan of ISTS 1809p Project (Delivery Event #6

Supplement 2 to the Work Plan

Deliverables Event/Activity	Expected Completion Date	
1. Seminar	the 3rd month of the 1st Quarter	+
2. Interim Report 1	the 1st month of the 2nd Quarter	+
3. Seminar/Conference	the 3rd month of the 2nd Quarter	+
4. Interim Report 2	the 1st month of the 3rd Quarter	+
5. Seminar/Conference	the 3rd month of the 3rd Quarter	+
6. Final Report	the 3rd Month of the 4th Quarter	+

Project Team

Bityurin Valentin Anatol'evich	Dr., Concept and Solution approach
Bocharov Aleksey Nikolaevich	Dr., Numerical Simulation
Leonov Sergey Borisovich	Dr., Experimental Methods
Baranov Dmitrii Sergeevich	Dr., Experimental facility assemblage
Kolpakov Andrei Vladimirovich	Dr., Non-equilibrium plasma Simulation

At different stages of investigation a credit was made by:

Sukhov Valeriy Nikolaevich	Scheme of the Experiment
Potebnya Vladislav Grigor'evich	Numerical Simulation
Bocharova Elena Anatol'evna	Data Treatment
Semenova Tat'yna Mikhailovna	Publication

I. INTRODUCTION

One of the main problems of stable combustion in high-speed flow is an effective mixing of gaseous fuel and oxidant providing full combustion during the resident time in combustor chamber. Generally speaking in-flow mixing consists of two main mechanisms: kinematics mixing (convection) and molecular diffusion. The latter is a final stage of mixing needed to provide extended combustible mixture. Kinematics mixing is more effective in vortex flows; the higher vorticity the better kinematics mixing which means the larger fuel/oxidant interface surface. The second mixing mechanisms – diffusion forms a *reacting volume* estimated as the interface surface times *diffusion length.* The only place where the combustion can occur is the *reacting volume.* Both *interface surface* and *diffusion length* are increasing functions of time. Having these two functions explicitly one can calculate a *reacting volume* formation and, with chemical kinetics scheme known, the combustion process can be described in detail. Such an approach has been developed in IVTAN for simulation of high-speed flow of chemically reacting mixture for plasma chemistry applications and simulation of combustion in compressor-type chemical reactors basing on Diesel engine.

Because very short residence time is typical of ram/scram jet operation conditions the measures providing a significant increasing rate of *reacting volume* are very actual.

The proposed Advanced Mixing approach is to increase the reacting volume growth by (1) pulse electrical discharge and (2) by MHD interaction - $\mathbf{J}\acute{}\,\mathbf{B}$ body force.

It was found recently both experimentally and theoretically that under certain conditions typical of so called Plasma Aerodynamics experiments the filamentary structure of high frequency discharge (streamer discharge) results sometimes in high speed jet formation. Such a jet can transfer a significant mass of fluid from one point to another rather distant location. Thus, providing a controllable filamentary discharge across a primary fuel/oxidant interface one can intensify the initial mixing of fuel/oxidant composition.

The second component of Advanced Mixing is vortex generation by a highly non-potential $\mathbf{J}\acute{}\,\mathbf{B}$ body force. This force is defined by current density component $\mathbf{J}_{\wedge}$ perpendicular to the external applied magnetic field **B.**

The preliminary information about such a mixing process was collected in IVTAN while an MHD generator flow with current-currying non-uniformities was studied. At that time the main question was how to decrease the mixing process intensified by vorticity generation. Now the amplification of mixing by MHD and Pulse Plasma affects should be studied in turn and recommended.

In practice the formation of reacting volume is provided, the first – by diffusion, which is rather conservative and under conditions of interest slow process, and, the second – by kinematics mixing. The latter can be very intensive due to turbulence generated at the unstable interface of free jet in a resting media. However, even in such a case the significant length is needed to provide kinematics pre-mixing of whole fuel-oxidizer mass flow. Furthermore, the kinematics pre-mixing resulting in a multi-scale irregular fuel-oxidizer structure consisting of stretched and deformed original pure fuel and oxidizer volumes is not yet enough to provide a combustion conditions. Only diffusion leads to a combustible mixture formation. The role of kinematics mixing is to reduce of characteristics scale (thickness) of inter-component stratified structure. It seems that the kinematics mixing stage required for the preparation of a combustible mixture is defined by the condition when the stratified system characteristics length l_S is comparable with the diffusion length. The diffusion length time evolution can reliably be estimated with a square root law. Thus, the diffusion time required for the desirable mixing is estimated as $t_D \sim l_S{}^2/D$. For a rum jet combustor applications this estimation is followed by the condition that requires the mixing time to be less than the residence time $t_R \sim L_C/V_C$ with L_C and V_C stand for the combustor length and in-combustor velocity, correspondingly. Thus, the practical situation analysis came back to the study of fundamental problem proposed for this project – the Advanced mixing utilizing non-mechanical mechanisms to intensify the reacting volume creation. The additional problem related to feature is to check the possible effects of electric field on the kinetics of combustion and, in particularly, on the ignition. The expected effect is to improve (accelerate) the ignition stage due to non-thermal formation of active radicals by the strong electric field applied or arisen in the flow through MHD interaction. Such an extra thermal formation of the radicals (e, O, O^+, OH, OH^-, and others) can be provided by the electric field directly in ionization and dissociation induced by electron-molecule collisions.

It is clearly seen from above brief description of the process considered here that the very sophisticated physical and mathematical models are needed to treat these phenomena at acceptable accuracy. From the other hand, not all input data required for the closed formal description are available, and for this reason the experimental validation is absolutely necessary.

Basing on the preliminary results of analysis conducted in the frame of the preceding work under contract with EOARD [1] the approach of this study consists of: (1) – the mathematical model development utilizing the full Navier-Stokes equation, reduced Maxwell equation to treat the MHD interaction process, and the chemical kinetics solver with a appropriate chemical kinetics scheme; (2) – parametric study with the numerical model developed; and (3) – the experimental setup design development. In order to reduce the computational time defined mainly by the

chemical kinetics scheme used in this study a rather compact scheme of hydrogen-oxygen combustion is applied.

In fact the main theoretical and numerical models needed have been developed earlier. In the present work the following physical effects are of primary interest:

a) Molecular viscosity and heat conductivity. The turbulence effects are hoped to be resolved directly rather then via some turbulence model. Most of turbulence models are capable of describing the mean flow only if the flow is stationary or the flow field varies slowly. We shall consider the earlier stages of mixing process, when undeveloped turbulence may exist. At this stage we consider originally undisturbed flow stage, therefore the only mechanism of mixing seems to be the molecular transport.

b) Multi-component diffusion. Traditional approach to the diffusion of particles in multi-component mixtures will be applied in this work. It is assumed that the diffusive flux of any species is proportional to the local gradient of its concentration (Fick's law). The baro-diffusion and thermo-diffusion fluxes can be neglected in the flows under consideration.

c) Magneto-hydrodynamic interaction. This is the main effect driving the flow. The arc-wise plasma formation can be created either in fuel or oxidizer and sustained due to external electric source. The arc current interacts with the transversal magnetic field so that the arc moves toward the fuel-oxidizer interface and enhances stirring of components. For the goals of the work the quasi-steady approach to MHD-interaction is certainly applicable: the characteristic speeds of the processes under consideration are much smaller compared to speed of light. In addition, the induced magnetic field due to electric currents can be neglected, so the current flow under constant external magnetic field can be considered. The approach to description of plasma properties, of which the electrical conductivity is of primary importance, is as follows. We expect that for low-temperature (several thousand degrees of Kelvin) poorly ionized plasma the approximations based on the Saha-equilibrium model are reasonable; so that the conductivity can be considered as the function of gas temperature. Same, in principal, could be valid for so-called Hall parameter. The radiation from the plasma will be taken into account via approximation of radiative power as function of temperature.

d) Finite-rate chemistry. For the reacting flow computations we shall apply a general finite-rate chemistry approach, based on the solution of chemical kinetics equations to obtain the species rates of production at each spatial point. Any chemical reaction is assumed to subject to the acting-mass law and reaction rate constants are assumed to be of Arrhenius type.

In this report, the mathematical model including the complete set of governing equations is presented in Section II, the computational model and solution algorithm are described in Section III. Specific features of the numerical experiment setup are discussed in Section IV. The main results of parametric study are presented in Section V. The initial stage of experimental facility development is briefly described in Section V. The summary of this study is presented in the Concluding Remarks.

II. MATHEMATICAL MODEL

The flows under consideration can be described by the coupled system of two-dimensional equations reflecting the conservation of mass, momentum and total energy for the whole mixture (Navier-Stokes equations), conservation of mass of different species with taking in to account the chemical conversions. The system is enclosed by the equations of state, by definition of transport coefficients, by definitions of chemical rates of productions for every species and by relationships describing the electromagnetic interaction. Below, the general mathematical model is given as it is implemented in the code.

$$\frac{\partial \mathbf{U}}{\partial t}+\frac{\partial \mathbf{F}}{\partial x}+\frac{\partial \mathbf{G}}{\partial y}+\frac{\partial \mathbf{F}_v}{\partial x}+\frac{\partial \mathbf{G}_v}{\partial y}=\mathbf{S} \quad , \tag{1}$$

U is the conservative-variable vector,

$$\mathbf{U}=\begin{pmatrix} \rho \\ \rho v_x \\ \rho v_y \\ \rho E \\ \rho Y_1 \\ \vdots \\ \rho Y_N \end{pmatrix} \tag{2}$$

where ρ is the fluid density, v_x and v_y are the velocity components, E is the total specific energy, and $\{Y_i, i=1,N\}$ are the species mass-fractions, $Y_i=\rho_i/\rho$, $\sum_{i=1}^{N} Y_i \equiv 1$.

The *inviscid flux-vectors* are given as

$$\mathbf{F}=\begin{pmatrix} \rho v_x \\ \rho v_x^2+P \\ \rho v_x v_y \\ v_x \rho E+v_x P \\ \rho v_x Y_1 \\ \vdots \\ \rho v_x Y_N \end{pmatrix}, \mathbf{G}=\begin{pmatrix} \rho v_y \\ \rho v_x v_y \\ \rho v_y^2+P \\ v_y \rho E+v_y P \\ \rho v_y Y_1 \\ \vdots \\ \rho v_y Y_N \end{pmatrix} \tag{3}$$

Here, P thermodynamic pressure defined later.

Diffusive fluxes are described as follows:

$$\mathbf{F}_v = \begin{pmatrix} 0 \\ \tau_{xx} \\ \tau_{xy} \\ e_x \\ J_{x1} \\ \vdots \\ J_{xN} \end{pmatrix}, \qquad \mathbf{G}_v = \begin{pmatrix} 0 \\ \tau_{xy} \\ \tau_{yy} \\ e_y \\ J_{y1} \\ \vdots \\ J_{yN} \end{pmatrix} \tag{4}$$

The components of viscous stress tensor:

$$\begin{aligned} \tau_{xx} &= -2\mu \frac{\partial v_x}{\partial x} + \frac{2}{3}\mu \nabla v, \\ \tau_{xy} &= \tau_{yx} = -\mu\left(\frac{\partial v_x}{\partial y} + \frac{\partial v_y}{\partial x}\right), \\ \tau_{yy} &= -2\mu \frac{\partial v_y}{\partial y} - \frac{2}{3}\mu \nabla v \end{aligned} \tag{5}$$

where μ is the molecular viscosity, $\nabla v = \frac{\partial v_x}{\partial x} + \frac{\partial v_y}{\partial y}$. The Stokes' hypothesis on the second viscosity has been taken into account in (5).

Energy fluxes are specified as:

$$\begin{aligned} e_x &= -\lambda \frac{\partial T}{\partial x} + \left(v_x \tau_{xx} + v_y \tau_{xy}\right) + \sum_{i=1}^{N} h_i J_{xi} \\ e_y &= -\lambda \frac{\partial T}{\partial y} + \left(v_x \tau_{xy} + v_y \tau_{yy}\right) + \sum_{i=1}^{N} h_i J_{yi} \end{aligned} \tag{6}$$

Here, λ is the heat conductivity and T is the temperature. The last terms in (6) represent the enthalpy fluxes due to multi-component diffusion.

Diffusive fluxes are defined according to Fick's law:

$$J_{xi} = -\rho D_{im} \frac{\partial Y_i}{\partial x} \quad , \quad i=1,N$$

$$J_{yi} = -\rho D_{im} \frac{\partial Y_i}{\partial y} \quad , \quad i=1,N \qquad (7)$$

Transport coefficients D_{im}, m, l.

$$D_{im} = (1 - X_i) \Big/ \sum_{j \neq i}^{N} X_j / D_{ij} \quad , \qquad (8)$$

$X_i = W \cdot Y_i / W_i$ is the mole fraction of i-th species, W_i is the molecular weight of i-th species and $W = 1 \Big/ \sum_{i=1}^{N} Y_i / W_i$ is the molecular weight of mixture. The binary diffusion coefficients, D_{ij}, are defined as follows:

$$D_{ij} = 2.68 \cdot 10^{-7} \frac{T^{3/2} \sqrt{(W_i + W_j)/(2W_i W_j)}}{P \cdot \sigma_{ij}^2 \cdot \Omega_{ij}^{(1.1)}(T_{ij}^*)} \quad \left[\frac{m^2}{s} \right] \qquad (9)$$

Here, $\sigma_{ij} = \frac{1}{2}(\sigma_i + \sigma_j)$ represent the characteristic collision diameter, $T_{ij}^* = kT/\varepsilon_{ij}$ (k is Boltzman constant) is the characteristic temperature, $\varepsilon_{ij} = \sqrt{\varepsilon_i \cdot \varepsilon_j}$ is the parameter of function describing the inter-molecular interaction.

Collision integral $\Omega_{ij}^{(1.1)}(T_{ij}^*)$ is approximated as $\Omega_{ij}^{(1.1)} = 1.074 \cdot (T_{ij}^*)^{-0.1604}$.

Viscous coefficient, μ, is calculated as

$$\mu = \sum_{i=1}^{N} \mu_i \left(1 + \sum_{j \neq i} G_{ij} \cdot \frac{X_j}{X_i} \right)^{-1} \qquad (10)$$

where i-th species viscous coefficient is defined as

$$\mu_i = 2.6693 \cdot 10^{-6} \frac{T^{3/2}\sqrt{W_i \cdot T}}{\sigma_i^2 \cdot \Omega_i^{(2.2)}(T_i^*)} \quad \left[\frac{kg}{m \cdot s}\right] \tag{11}$$

Collision integral $\Omega_i^{(2.2)}(T_i^*)$ is approximated as $\Omega_i^{(2.2)} = 1.157 \cdot (T^*)^{-0.1472}$, and functions G_{ij} are defined as

$$G_{ij} \frac{\left[1 + \left(\mu_i / \mu_j\right)^{1/2} \left(W_i / W_j\right)^{1/4}\right]^2}{2^{3/2}\left[1 + W_i / W_j\right]^{1/2}}$$

The heat conductance coefficient is defined as follows:

$$\lambda = \sum_{i=1}^{N} \lambda_i' \left(1 + 1.065 \sum_{j \neq i} G_{ij}' \cdot \frac{X_j}{X_i}\right)^{-1} \tag{12}$$

where $\lambda_i' = \lambda_i \left(0.115 + 0.354 \cdot C_{pi} / R_i\right)$

functions G_{ij}' are defined as

$$G_{ij}' \frac{\left[1 + \left(\lambda_i / \lambda_j\right)^{1/2} \left(W_i / W_j\right)^{1/4}\right]^2}{2^{3/2}\left[1 + W_i / W_j\right]^{1/2}}$$

i-th species heat conductivity is defines as

$$\lambda_i = \frac{5}{2} \mu_i c_{vi}, \; c_{vi} = \frac{3}{2} \cdot \frac{R^0}{W_i} \tag{13}$$

R^0 is the universal gas constant, R_i is the gas constant of i-th species, $R_i = R^0/W_i$, c_{vi} and c_{pi} are species heats at constant volume and constant pressure, respectively.

Thermodynamic properties of mixture.

Equation of state

$$P = \rho R \cdot T \tag{14}$$

where P is the pressure, T is the temperature, R is the gas constant, $R=R^0/W$.

Caloric relation

$$e = h - P/\rho \tag{15}$$

where e is the specific internal energy and h is the specific enthalpy. Total energy is defined as

$$E = e + \frac{1}{2}\left(v_x^2 + v_y^2\right) \tag{16}$$

and

$$h = \sum_{i=1}^{N} Y_i h_i(T) \tag{17}$$

i-th species enthalpy, $h_i(T)$, is expressed as

$$h_i(T) = h_{i,f} + \int_{T_{ref}}^{T} c_{pi}(T)\, dT \tag{18}$$

where $h_{i,f}$ is the formation enthalpy of i-th component.

The source-term vector **S** is given as

$$\mathbf{S} = \begin{pmatrix} 0 \\ S_x \\ S_y \\ S_e \\ \dot{w}_1 \\ \vdots \\ \dot{w}_N \end{pmatrix} \tag{19}$$

Here, S_x and S_y represent the components of electro-magnetic force, S_e represents the energy rate of change due to Joule heating and radiation. These terms are described in the sub-section "Plasma Model" below. The terms $\{\dot{w}_i\}$, i=1,N represent the rates of production of species due to chemical reactions. They are described in "Finite-Rate Chemistry Model".

Plasma Model.

In general, the electrodynamics of steady-state weekly-ionized gas discharge can be described by Ohm's law:

$$\mathbf{j} + \frac{\beta}{B}[\mathbf{j} \times \mathbf{B}] = \sigma(\mathbf{E} + [\mathbf{v} \times \mathbf{B}]) \tag{20}$$

where **j** is the electric current density, **E** is the electric field strength, σ is the electric conductivity, **B** is the magnetic field induction, and β is the Hall parameter.

The components of electro-magnetic force are defined as

$$S_{x,y} = [\mathbf{J} \times \mathbf{B}]_{x,y} \tag{21}$$

Energy rate of change is

$$S_e = (\mathbf{J} \cdot \mathbf{E}) - Q_{rad}$$

where approximation to the radiative power Q_{rad} is taken in the form:

$$Q_{rad} = \varepsilon \cdot \sigma_{SB} \cdot T^4 \ , \qquad (23)$$

where ε is the effective absorption coefficient, and σ_{SB} is the Stefan-Boltzman constant.

Coupled with the definition of electric potential, **E**=-grad φ, the Equ(20) can be reduced to single two-dimensional (three-dimensional in general) equation for potential.

Finite-Rate Chemistry Model

The chemical kinetics model is applied to determine the species rates of production $\{\dot{w}_i\}$ due to chemical conversions, or reactions.

Any chemical reaction can be represented symbolically as:

$$\sum_{l=1}^{N} \nu'_{l,r} X_l \quad \underset{k_{fb}}{\overset{k_{fr}}{\rightleftharpoons}} \quad \sum_{l=1}^{N} \nu''_{l,r} X_l \qquad (24)$$

where $\nu'_{l,r}$ and $\nu''_{l,r}$ are the stoichiometric coefficients of reagents and products, respectively.

The *i*-th species rate of production is then defined in accordance with the acting-mass law:

$$\dot{w}_i = W_i \sum_{r=1}^{N_r} \left[\nu''_{i,r} - \nu'_{i,r}\right] \cdot \left(k_{fr} \prod_{l=1}^{N} c_l^{\nu'_{l,r}} - k_{br} \prod_{l=1}^{N} c_l^{\nu''_{l,r}} \right) \qquad (25)$$

Here, $c_l = \rho \cdot Y_i / W_i$ are the molar concentrations. k_{fr} and k_{br} are the reaction rate constants, forward and backward, respectively. The Arrhenius form is assumed for both k_{fr} and k_{br}:

$$k_{fr} = a \cdot T^b \cdot \exp\left(-E_a / T\right) \qquad (26)$$

where *a,b* and E_a are reaction parameters. These can be evaluated theoretically or from experimental data. For the hydrogen-air mixture these data are tabulated as well as that for many other reactions.

The first stage study with the model described above has concerned the feasibility of the electric arc to initiate and maintain the combustion via the motion across the fuel/oxidizer interface due to electromagnetic field. It was numerically shown that such a discharge both initiates combustion process in the mixing layer due to high temperature of the arc and increases the mixing/combustion volume due to arc motion and enhanced diffusion of species in the volume. The combustion was detected to be self-sustained during rather long time even the current and/or magnetic field is switched off.

In those computations rather simple models of the medium were used.

First, the chemical kinetics mechanism used is considered to be appropriate to the combustion under thermal equilibrium. In addition, the kinetics under temperatures higher than 3000K can differ from that considered before. Therefore sophisticated kinetic scheme should be tested which includes interactions with the charged particles, first of all, electrons. The neutral-neutral interactions should be revised for temperatures higher than 3000K.

Second, the transport properties of the multi-component mixture should be revised due to availability of electric field and charged particles. First of all the conductivity of plasma should be computed more accurately. The electron-neutral and electron-ion collisions are of importance. In general these interactions depend upon electron concentration and electron temperature, the latter being different from heavy particles temperature. Other transport properties such as viscosity, heat conductivity and diffusion coefficients can significantly be effected by the charged particles interactions. Moreover, the approach to mass-diffusion used up so far should be re-evaluated. This approximate approach is based on the Fick's law and effective diffusion coefficients. The approach is known to be stable while time-integration, but may be inadequate in plasmas with the deep property gradients. In this case the solution Stefan-Maxwell equations may become necessary.

Third, the radiation emission from the discharge region was estimated with the approximate model. It was assumed that total radiation losses from optically thin plasma can be calculated by simple law taking into account the local absorption coefficient. Special study is still needed to understand whether the radiation losses are important from the viewpoint of energy balance. If so, they should be evaluated with more sophisticated model.

The following sections are primarily intended to analyze the plasma models used before and to select the models more suitable for the discharges under consideration. Three items will be analyzed below: chemical kinetics, transport properties and radiation losses.

In Table 1 a typical chemical kinetics scheme is presented. This scheme was used in the first series of numerical simulation.

Table 1. List of reactions for H_2-O_2 combustion

1) $H_2 + O_2 \Leftrightarrow OH + OH$
2) $OH + H_2 \Leftrightarrow H_2O + H$
3) $H + O_2 \Leftrightarrow OH + O$
4) $O + H_2 \Leftrightarrow OH + H$
5) $O + H_2O \Leftrightarrow OH + OH$
6) $H + H + M \Leftrightarrow H_2 + M$
7) $H + O_2 + M \Leftrightarrow HO_2 + M$
8) $OH + H + M \Leftrightarrow H_2O + M$
9) $HO_2 + H_2 \Leftrightarrow H_2O_2 + H$
10) $HO_2 + HO_2 \Leftrightarrow H_2O_2 + O_2$
11) $H + HO_2 \Leftrightarrow OH + OH$
12) $H + HO_2 \Leftrightarrow H_2O + O$
13) $H + HO_2 \Leftrightarrow H_2 + O_2$
14) $O + HO_2 \Leftrightarrow OH + O_2$
15) $OH + HO_2 \Leftrightarrow H_2O + O_2$
16) $OH + OH + M \Leftrightarrow H_2O_2 + M$
17) $HO_2 + H_2 \Leftrightarrow H_2O + OH$
18) $HO_2 + H_2O \Leftrightarrow H_2O_2 + OH$
19) $H + H_2O_2 \Leftrightarrow H_2O_2 + OH$
20) $OH + M \Leftrightarrow O + H + M$
21) $O + O + M \Leftrightarrow O_2 + M$

It takes into account all main stages of the combustion process: excitation, ignition and heat release stage. The mixture is assumed to be in local thermal equilibrium.

However, under plasma conditions, the electron-impact reactions may play the significant role. For this reason the first simple chemical kinetics scheme of Table 1 is now reconsidered to be fit to the conditions of the experiments planned for future study.

The following interactions are planned to be included in the scheme.

1) Dissociation reactions

$$H_2 + e \Leftrightarrow H + H + e$$
$$O_2 + e \Leftrightarrow O + O + e$$
$$OH + e \Leftrightarrow O + H + e$$

2) Major ionization reactions

$$H_2 + e \Leftrightarrow H_2^+ + e + e$$
$$O_2 + e \Leftrightarrow O_2^+ + e + e$$
$$H + e \Leftrightarrow H^+ + e + e$$
$$O + e \Leftrightarrow O^+ + e + e$$
$$OH + e \Leftrightarrow OH^+ + e + e$$

This set of reactions is thought to be important on any stage of the combustion process. The data on these reactions are now being sought in the literature. The role of direct dissociation/ionization of water is now investigated. Interactions of electrons with several intermediate species like HO_2, H_2O_2 will probably be neglected since their life-time is rather small as well as their concentrations.

Ionization of main species due to neutral-neutral collisions of type of

$$X + M \rightarrow X^+ + M + e$$

where denotes H_2, O_2, O, H, OH, and M denotes any of the species will probably be not considered since such reactions occur under high temperatures (probably higher that 1eV). At the same time electron-impact reactions may take place due to high electron temperatures, which, in turn, may take place in high electric-field-strength discharge. Therefore, the set of dissociation/ionization reactions formulated above should depend on the electron temperature.

Another aspect of the scheme being developed arises from consideration of higher-temperature range. Within the arc, the temperatures higher than 3000K may occur. Hence, the dissociation reactions of type of

$$H_2 + M \Leftrightarrow H + H + M$$

which were included in the previous scheme may occur with the reaction rates different from those considered before. The preliminary list of reactions which are assumed to be included in the kinetic scheme is given in Table 2.

Table 2. Suggested list of reactions for H_2-O_2 combustion with ionization

1) $H_2 + e \Leftrightarrow H + H + e$
2) $O_2 + e \Leftrightarrow O + O + e$
3) $OH + e \Leftrightarrow O + H + e$
4) $H + e \Leftrightarrow H^+ + e + e$
5) $O + e \Leftrightarrow O^+ + e + e$
6) $OH + e \Leftrightarrow OH^+ + e + e$
7) $H_2 + e \Leftrightarrow H_2^+ + e + e$
8) $O_2 + e \Leftrightarrow O_2^+ + e + e$
9) $H_2 + O_2 \Leftrightarrow OH + OH$
10) $OH + H_2 \Leftrightarrow H_2O + H$
11) $H + O_2 \Leftrightarrow OH + O$
12) $O + H_2 \Leftrightarrow OH + H$
13) $O + H_2O \Leftrightarrow OH + OH$
14) $H + H + M \Leftrightarrow H_2 + M$
15) $H + O_2 + M \Leftrightarrow HO_2 + M$
16) $OH + H + M \Leftrightarrow H_2O + M$
17) $HO_2 + H_2 \Leftrightarrow H_2O_2 + H$
18) $HO_2 + HO_2 \Leftrightarrow H_2O_2 + O_2$
19) $H + HO_2 \Leftrightarrow OH + OH$
20) $H + HO_2 \Leftrightarrow H_2O + O$
21) $H + HO_2 \Leftrightarrow H_2 + O_2$
22) $O + HO_2 \Leftrightarrow OH + O_2$
23) $OH + HO_2 \Leftrightarrow H_2O + O_2$
24) $OH + OH + M \Leftrightarrow H_2O_2 + M$
25) $HO_2 + H_2 \Leftrightarrow H_2O + OH$
26) $HO_2 + H_2O \Leftrightarrow H_2O_2 + OH$
27) $H + H_2O_2 \Leftrightarrow H_2O_2 + OH$
28) $OH + M \Leftrightarrow O + H + M$
29) $O + O + M \Leftrightarrow O_2 + M$

Transport properties

In the previous work the transfer of species, viscous momentum and heat was modeled by the well-known multi-component diffusion model formulated in [2]. Commonly used simplification of

multi-component diffusion applied the effective diffusion coefficients and Fick's law to estimate species mass-flux was implemented in the code. All transport coefficients were estimated with using so called collision-integrals of viscous and diffusion types. In turn, the collision-integrals are obtained by integration of collision cross-sections over the energy space. The values of collision-integrals, $\Omega(l,s)$, were taken as approximations of temperature functions [3]. These approximations used the Lennard-Jones interaction potential to obtain the deflection angle of the colliding particles as function of impact parameter and relation energy, then the relevant cross section, and, finally, the collision integrals. The Lennard-Jones interaction potential model is known to work well for temperatures below nearly 1000K. At higher temperatures another models should be used for interaction potential. In addition, the interaction of charged particles should take into account the screened Coulomb potential.

Another aspect of the problem is related to using the Fick's law for mass-flux expression. It is easy to implement into the code, but the accuracy of the approach remains under question. More relevant, although time-consuming, is the solution of Stefan-Maxwell relations for mass-diffusion fluxes. The set of Stefan-Maxwell equations can be expressed as

$$\nabla x_i = \frac{M}{\rho}\sum_{j\neq i}\left(\frac{x_i J_j}{M_j D_{ij}} - \frac{x_j J_i}{M_i D_{ij}}\right), \text{ i=1, N-1} \qquad (27)$$

$$\sum J_j = 0$$

where J_i is the mass-flux of species i due to diffusion (only concentration diffusion is taken into account), x_i is the mole fraction of species i, M_i is the molecular weight of i-th species and D_{ij} are the binary diffusion coefficient. System (27) should be resolved for J_i. This requires matrix inverting, $\mathbf{J} = \tilde{D}^{-1}(\nabla \mathbf{x})$, which is extremely costly. Therefore, iterations are usually applied to obtain J_i. Nevertheless, this procedure still remains expensive compared with simplified models. Probably one of the best from the viewpoint of cost-accuracy consideration is the Yos model. The model gives diffusion flux of species i as

$$J_i = -\rho\frac{M_i}{M}\left(\frac{1-c_i}{1-x_i}\right)D_{im}\nabla x_i \qquad (28)$$

$$D_{im} = \frac{1-x_i}{\sum_{j\neq i} x_j / D_{ij}}$$

Here D_{im} is the effective diffusion coefficient, c_i is the mass-fraction of species *i*.

In the case of Stefan-Maxwell relations the driving force can take electric force into account directly. In Yos model it is neglected. Regardless of the diffusion model, the binary diffusion coefficients have to be calculated. Their calculation requires the knowledge of collision integrals. Two approaches are planned to try for collision-integral calculations.

First, collision-integral for neutral-neutral collisions $\Omega_{ij}^{(1.1)}$ is approximated as function of temperature: $\Omega_{ij}^{(1.1)} = \left(a_{ij} + b_{ij} \ln T\right)^2$, where parameters a_{ij} and b_{ij} can be found from known values of $\Omega_{ij}^{(1.1)}$ (T1=300K) and $\Omega_{ij}^{(1.1)}$ (T2=20000K) and assuming that Lennard-Jones interaction potential is valid at low temperatures,

$$\varphi_{ij} = 4\varepsilon_{ij}\left[\left(\frac{\sigma_{ij}}{r}\right)^{12} - \left(\frac{\sigma_{ij}}{r}\right)^{6}\right].$$

At high temperatures Born-Mayers potential $\varphi_{ij}(r) = A_{ij}\exp\left(-\alpha_{ij}\cdot r\right)$ is used. Ion-neutral collision-integrals can be calculated using empirical correlations [4,5]:

$$\Omega_{A^{\pm},N}^{(1.1)} = f(T)\cdot\Omega_{A,N}^{(1.1)}$$

$$f(T) = 1 + \left(\frac{1150}{T+600}\right)^2$$

Collision-integral of electron with any neutral particle is assumed to have constant value of 4Å^2 [6].

Interactions of charged particles are described with using screened Coulomb potential:

$$\varphi(r) = \frac{1}{4\pi\varepsilon_0}\frac{e_i e_j}{r}\exp\left(-r/r_D\right),$$

where $r_D^2 = \dfrac{\varepsilon_0 kT}{n_e e^2}$ is the Debay length.

The following approximations are assumed [4]:

$$\Omega_{++}^{(1.1)} = 0.523 r_L^2 \ln\left(1 + 0.6\Lambda\right) \text{ [Å}^2\text{]},$$

$$\Omega_{+-}^{(1.1)} = 0.405 r_L^2 \ln(1+2\Lambda) \ [\text{Å}^2],$$

if $1 \le \Lambda \le 100$

and

$$\Omega_{++}^{(1.1)} = \Omega_{+-}^{(1.1)} = 0.5 r_L^2 (\ln \Lambda - 0.305),$$

if $\Lambda > 100$.

Here

$$r_L^2(T) = \left(\frac{e^2 z_1 z_2}{4\pi\varepsilon_0 kT} \right)^2 \ [\text{Å}^2],$$

$$\Lambda(T, n_e) = \frac{r_D}{r_L} = A \frac{T^{3/2}}{n_e^{1/2}}.$$

To calculate viscosity and heat conductivity we plan to use approximations of type of Wilke-Vasil'eva [7]:

$$\mu = \sum_{i=1}^{N} c_i \frac{Sc_i}{d_i}$$

$$\lambda = \sum \frac{c_i}{M_i} \left[c_{pi} + 2.5 R^0 (1.5 Sc_i - 1) \frac{1}{d_i} \right]$$

where

$$d_i = \sum_j \frac{c_j}{M_i D_{ij}}$$

The Schmidt number $Sc_i(T) = \frac{5\Omega_{ii}^{(1.1)}}{6\Omega_{ii}^{(2.2)}}$. It is assumed that $\Omega_{ii}^{(2.2)} = 1.1 \cdot \Omega_{ii}^{(1.1)}$ for all components. Some data were also taken from [8].

In second approach the collision-integrals values can be taken in closed form as functions of temperature [9]. In this work the collision-integrals were calculated for many equilibrium air species interaction including the charged particles interactions.

In the future it is assumed to implement both transport coefficients models to take into account charged particles interactions.

Radiation from plasma

In the calculations made earlier the simplest radiation model was used. The model used the concept of “gray-body” with effective absorption coefficient. Such concept just estimates the level of radiation power, probably upper limit of it. Currently, we don’t know how accurate are these estimations. Detailed analysis of radiation emission is extremely complex problem, and it is hardly possible to do by ourselves. Nevertheless, work is now carried out to find acceptable level of radiative losses description.

Concluding remarks on the mathematical model development

The time period of last several months has been devoted to the analysis of the models applied to the investigations of MHD assisted mixing/combustion in non-premixed fuel/oxidizer system. From examination of the literature we drew a conclusion that some modifications and improvements should be made both in physical and computational models of the processes analyzed.

First, the kinetic mechanism should be corrected to take into account reactions with charged particles and to expand the model to higher temperature range. The preliminary list of reactions has been compiled, and now the work is done to implement it to the code and to test it.

Second, the transport properties models were analyzed since we think that the current model is not completely adequate to simulate the transfer in non-equilibrium system with the charged particles and strong property gradients. The most robust candidate seems to be the Stefan-Maxwell relations for mass-diffusion fluxes. At the same time this model is known to be rather costly from computational point of view. The compromise between cost and accuracy may be the Yos diffusion model. Both these models are now being implemented to the code and tested. Also modifications to the models of viscosity and heat conductivity are being introduced.

Third point of analysis carried out seems to be not so important compared to first two. Nevertheless some more sophisticated estimations of radiation losses from the arc are being worked out.

III. NUMERICAL METHOD

In order to obtain all flow fields in any point of the domain under consideration, the entire computational domain is divided onto small domains called cells. Within each computational cell, the flow variables may be assumed to be constant (first – order accurate solution) or, for example, to be linear (second – order accurate solution). Other cell-distributions are possible, but are extremely expensive from the viewpoint of computational time. Only constant and linear variable distributions are implemented in the code.

The system (1) is discretized in space and time starting from integral conservation laws (weak formulation):

$$\frac{\partial}{\partial t}\int_{\omega}\mathbf{U}\,d\omega+\int_{\partial\omega}\mathbf{F}\,dS_{\omega}=\int_{\partial\omega}\mathbf{F}_{v}\,dS_{\omega}+\int\mathbf{S}\,d\omega \qquad (29)$$

This is integral form of (1) valid for any computational cell with the volume ω enclosed by the surface S_ω (in two-dimensional case ω is the surface and S_ω is the curve surrounding the cell). For both constant and linear variable distribution-in-cell, the transient term in (29) can be approximated as follows:

$$\frac{\partial}{\partial t}\int_{\omega}U\,d\omega\cong\omega\cdot\frac{\Delta\mathbf{U}}{\Delta t},$$

where $\Delta U=U(t+\Delta t)-U(t)$ with the 1-st order approximation of time-derivate. The surface fluxes are integrated as follows. For example,

$$\int_{S_\omega}\mathbf{F}\,d\mathbf{S}_{\omega}=\int F\,dS_{\omega}^{x}+\int G\,dS_{\omega}^{y}=\int(Fn_{x}+Gn_{y})\,dS_{\omega}=\left\langle F\cdot n_{x}+G\cdot n_{y}\right\rangle\Delta S_{\omega} \qquad (30)$$

Here, ΔS_ω is the surface area value, n_x and n_y are the components of unit normal-vector directed outward the cell considered. The average-flux value depends on the grid partition and on the variable distribution-in-cell. We shall consider the quadrilateral cells, so that any internal computational cell has four neighbors. The relationships (30) are then rewritten as follows:

$$\int \mathbf{F}\, d\mathbf{S}_\omega = \sum_{j\in\omega} \int F\ dS_j \cong \sum_j F_j \Delta S_j$$

where F_j stands for the face-averaged flux and S_j stands for the face area. The face implies the line-segment, part of the whole cell-surface, straddling two adjusting cells. Four faces enclose each computational cell. For 1st- and 2nd order accurate solutions, the one-integration-point is sufficient, i.e. the surface flux can be evaluated at the mid-point of the face:

$$\int F_j dS_j \cong \mathbf{F}(\mathbf{U}_m)\Delta\mathbf{S}_j = \left\lfloor F(\mathbf{U}_m)n_x + G(\mathbf{U}_m)n_y \right\rfloor \Delta\mathbf{S}_j \qquad (31)$$

The flux components, F and G, were presented in the previous Section. The dissipative fluxes, F_v and G_v, are handled with analogously.

The source-term is discretized as follows

$$\int \mathbf{S}\, d\omega \cong \omega \cdot \mathbf{S}(\mathbf{U}_\omega)\ .$$

Hereafter, all the flow variables imply cell-volume-averaged,

$\int U\ d\omega = \omega \cdot \mathbf{U}_\omega$, or simply, $\omega \cdot \mathbf{U}$.

Collecting surface-flux integrations and giving variable distribution-in-cell leads to a system of algebraic non-linear equations for each cell state-vector **U**:

$$\omega \frac{\Delta \mathbf{U}}{\Delta t} + \mathbf{R} = 0 \quad (32)$$

where residual-vector **R** is the approximation of surface-flux quadratures plus source term:

$$\mathbf{R} = \sum_{j\in\omega} \left\lfloor F_j^{\Sigma}(\mathbf{U}_{mj})n_{xj} + G_j^{\Sigma}(\mathbf{U}_{mj})n_{yj} \right\rfloor \Delta S_j + \int \mathbf{S}\, d\omega \qquad (33)$$

The system (32) is integrated in time using explicit low-memory Runge-Kutta method:

$$\mathbf{U}_0 = \mathbf{U}^n$$

$$\mathbf{U}_i = \mathbf{U}_0 - \alpha_i \frac{\Delta t}{\omega}\mathbf{R}(\mathbf{U}_{i-1}) \quad , \quad i=1,I \tag{34}$$

$$\mathbf{U}^{n+1} = \mathbf{U}_I$$

where $\mathbf{U}^n$ is the solution on time-level t^n and $\mathbf{U}^{n+1}$ is the solution on time-level

$$t^{n+1} = t^n + \Delta t$$

The time-step, Δt, is selected as minimum of convective and diffusive time-scales for all the mesh control-volumes. While source-terms for momentum and energy equations are computed explicitly, calculation of chemical species production rates is carried out implicitly employing special chemical-kinetics solver.

$$\dot{w}_i = \left.\frac{d(\rho Y_i)}{dt}\right|_{chem} = \frac{1}{\Delta t}\int_{t^n}^{t^n+\Delta t} \dot{w}_i \, dt \tag{35}$$

Integration in time is performed by the program KINEL developed in IVTAN Low-Temperature Plasma Division for solution of systems of ordinary differential equations of high stiffness inherent to problems with chemical and thermal non-equilibrium. On every time-step, Δt, system (4c) is integrated based on “chemical” time-steps and implicit treatment of production-rates. The chemical time-steps are evaluated within KINEL on the base of eigen-values of chemical source-term Jacobian matrix. Low-cost LU-decomposition of Jacobian is applied on each chemical time-step to solve the system.

Implicit treatment of chemical source-term allows one to avoid strong restrictions to the gas-dynamic time-steps imposed by finite-rate chemistry.

The integration of inviscid and viscous flux-vector over the control-volume surface is performed as follows. One-integration-point on the each surface-element (cell-interface straddling two neighboring cells) is suitable to obtain both 1-st order solution (piece-wise constant variable distribution within the cell) and 2-nd order solution (piece-wise linear variable distribution) in space. The inviscid flux at the integration-point is found from exact solution of Riemann problem (Godunov’ method), i.e.

$$\mathbf{F}_{ip} = \mathbf{F}(\mathbf{U}_{ip}), \text{ and } \mathbf{U}_{ip} = Rie(\mathbf{U}_L, \mathbf{U}_R) \tag{36}$$

Rie($\mathbf{U}_L$, $\mathbf{U}_R$) implies solution of Riemann problem between two states $\mathbf{U}_L$ and $\mathbf{U}_R$, left and right state-vectors on both sides of the interface. For two adjacent cells, *P* and *E*,

$$\mathbf{U}_L = \mathbf{U}_P + \psi_P\left(\nabla\mathbf{U}_P, \Delta\mathbf{r}_{Pm}\right)$$
$$\mathbf{U}_R = \mathbf{U}_E - \psi_E\left(\nabla\mathbf{U}_E, \Delta\mathbf{r}_{Em}\right) \qquad (37)$$

$\nabla\mathbf{U}_{P,E}$ are the cell-centered gradients and Δr_{EM} is the vector directed from cell-center *P*(*E*) to mid-point of the interface M. The gradient in each cell, $\nabla\mathbf{U}_P$, is calculated by the least-square method as minimum of functional

$$\Phi_P = \sum_{J\in\omega_P}\left[\Delta U_{Pj} - \left(\nabla\mathbf{U}_P \cdot \Delta\mathbf{r}_{Pj}\right)\right]^2 \quad ,$$
$$\Delta U_{Pj} = \mathbf{U}_j - \mathbf{U}_P$$

Here *J* stands for any cell from the stencil associated with cell *P*. Usually, five-point stencil of the nearest neighbors (including *P*) is considered. The limiter-functions ψ_P's are taken to satisfy the monotonical distributions near the strong flow discontinuities. In the smooth-flow regions, the second-order accurate spatial distributions are recovered. In one-dimensional problem, this method becomes equivalent to the well-known Van Leer MUSCL method.

Viscous fluxes at cell interface may be constructed in two ways. In first way, the face-gradient is taken to be the algebraic average of two cell-gradients described just above with adding up the projection of normal-derivative to prevent the non-physical oscillations. In second way, the gradient at interface is calculated by application of Gauss' theorem to auxiliary cell

$$\omega_a(\nabla\mathbf{U}_M) = \int_{\partial\omega_a}\left(\mathbf{U}\cdot\mathbf{n}_a\right)dS_a \,.$$

Auxiliary cell represents the quadrilateral which vortices are two cell-centers (*P* and *E*) and start-point and end-point of the interface segment itself. Both approaches were found to be equally appropriate.

IV. PARAMETRIC STUDY

IV-1. Arc-Driven Mixing and Combustion

To highlight the main effects discussed in Introduction we consider a simplified problem. Assume that the rectangular parallelepiped is filled with separated air and hydrogen. Let the computational plane be the *XY*-plane. The size of the domain in *X*-direction is taken to be 10 mm. The size of the domain in *Y*-direction is also taken to be 10 mm. We assume that variations of the flow parameters in *Z*-direction can be neglected, so that the two-dimensional problem in *XY*-plane could be considered. The domain is filled with the separated fuel components in such a way that upper half of the domain ($Y>5$) is filled with air and lower half is filled with hydrogen. This will referred to as the Case 1. Alternate filling case, i.e. hydrogen if $Y>5$ and air if $Y<5$, will be referred to as the Case 2. At the initial moment the arc of 2 mm in diameter is ignited so that the center-point of the arc locates at the point x=5mm, y=3mm. The arc column is specified to be co-linear to *Z*-direction and is assumed to maintain from the external electric source. In all the calculations the total current through the arc 10 Ampere is assumed to hold. The constant magnetic field is specified as $\mathbf{B} = (B,0,0)$, $B = 2$ tesla. In such formulation the vectors of current density and electric field take the following form:

$\mathbf{J} = (0,0,J_z)$, $\mathbf{E} = (0,0,E_z)$.

The component of electric field vector E_z is the same everywhere in the domain. For simplicity, we neglect with the induced electric field, [**V´B**]. This can be done since the characteristic flow speeds of the order of 100 m/s were expected (and calculated), whereas the applied electric field varied in the range from 1 to 4 kV/m. Then, one can write for total current

$$I_{arc} = \int J_z \, dS_{xy} = \int \sigma \cdot E_z \, dS_{xy} = E_z \cdot \int \sigma \, dS_{xy}$$

$$E_z = I_{arc} \Big/ \int \sigma \, dS_{xy}$$

$$J_z = \sigma(x,y) \cdot E_z$$

Next, the electro-magnetic force has only one component, namely

$$S_x = J_z \cdot B, \; S_y = 0$$

The energy rate of change, S_e, is given by expression:

$$S_e = (\mathbf{J} \cdot \mathbf{E}) = J_z \cdot E_z$$

The following initial conditions are specified. Pressure P_0 = 105 Pa, temperature T_0 = 300K outside the arc and T_0 = 6000K inside the arc. The boundaries of the domain are considered to be the adiabatic walls.

Some results can be seen from Figures 1-3. In Fig.1, the no-chemistry Case 1 is presented. The distributions of mass fraction of hydrogen (left) and temperature (right) are shown for 8 time-moments. For the same time-moments, the same distributions are given in Fig.2 for Case 1 (with chemistry). Also, the main combustion product, H_2O, is shown by colored contours. Finally, Case 2 is represented in Fig.3.

The first observation, which immediately can be done, is that the region of disturbance of the original contact boundary is essentially higher for Case 1 compared to original arc diameter. The characteristic size of combustion zone is comparable with the size of the domain. The combustion zone is well detected by the water mass fraction distributions. The water mass fraction reaches the value of ~ 0.21 (maximum) at the final stage. The maximum temperature varies from ~ 5000K at 5mcs to 3900K at the final moment. Comparison of Fig.1 (no chemistry Case 1) with Fig.2 shows that mixing process is mainly due to arc motion. In both cases the electro-magnetic force is nearly the same, which determines the similar flow patterns. Although, some small differences exist: the disturbance zone is slightly larger for the reactive case, while the maximum temperature is in average higher for the non-reactive case.

The situation becomes quite different when arc is ignited in the air. In this case no essential mixing zone enhancement is observed, while temperature becomes as high as ~ 7200K. This is the fact that in the Case 1 the arc ignited in the light hydrogen and therefore moving quickly “strikes” with the heavy air, which acts like the wall. The flow reflects from the contact boundary rather then passes through it. This leads to smearing of the arc along the boundary and high diffusion (due to high temperatures) provides an initiation of combustion on a wide front. In opposite Case 2, slowly moving arc ignited in the heavy air begins to accelerate when coming into the light hydrogen. Therefore, the mixing zone surrounds the arc, which is as narrow as original one. In the Case 2, the maximum water concentration reaches the value of 0.1. It is clear that total water production is significantly higher in the Case 1. Even if one compares the flow patterns at the same time moments (35mcs), the more developed combustion zone in Case 1 is evident.

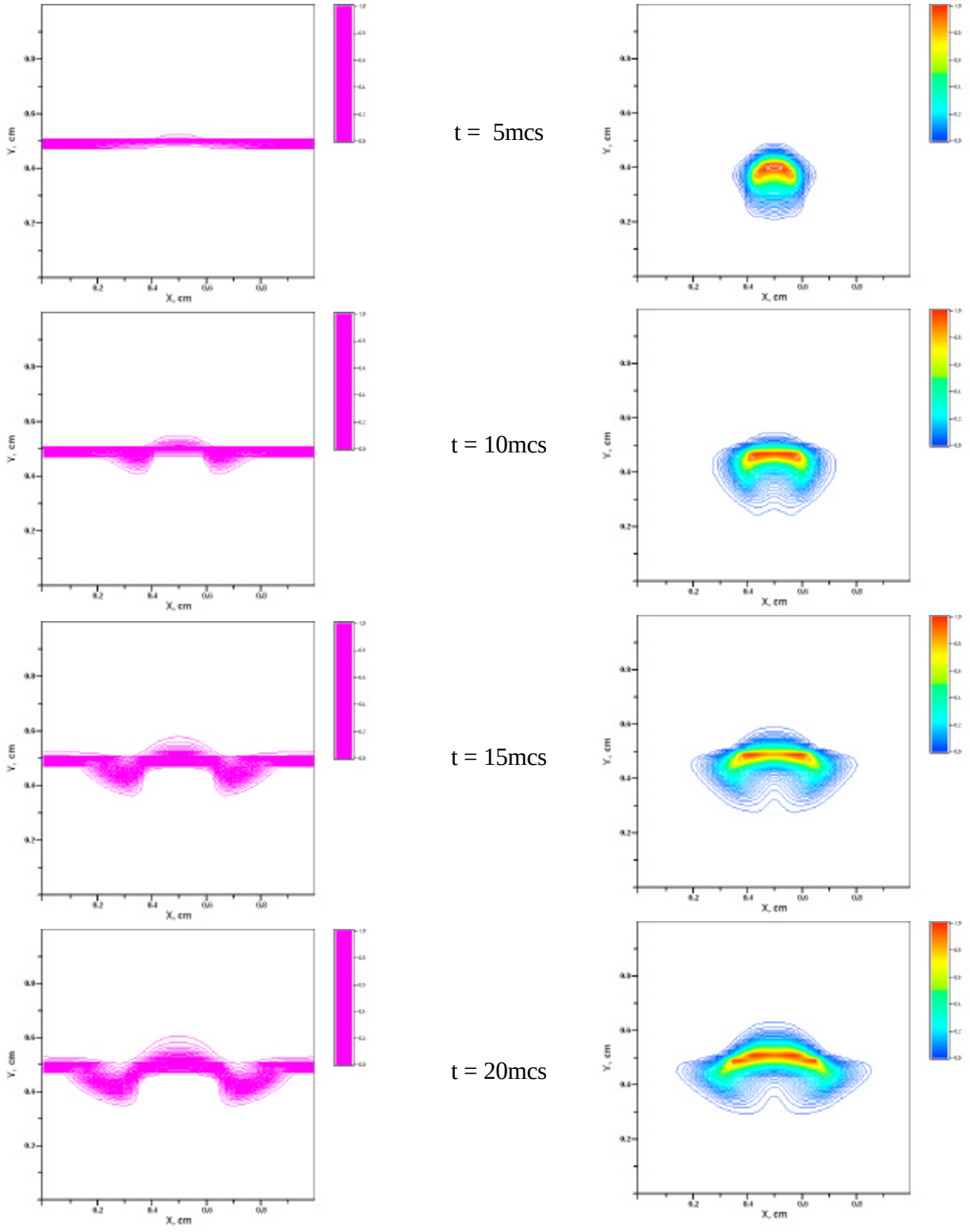

Fig.1. The mass fractions of hydrogen and water(left) and temperature(right) for Case 1 (no chemistry).

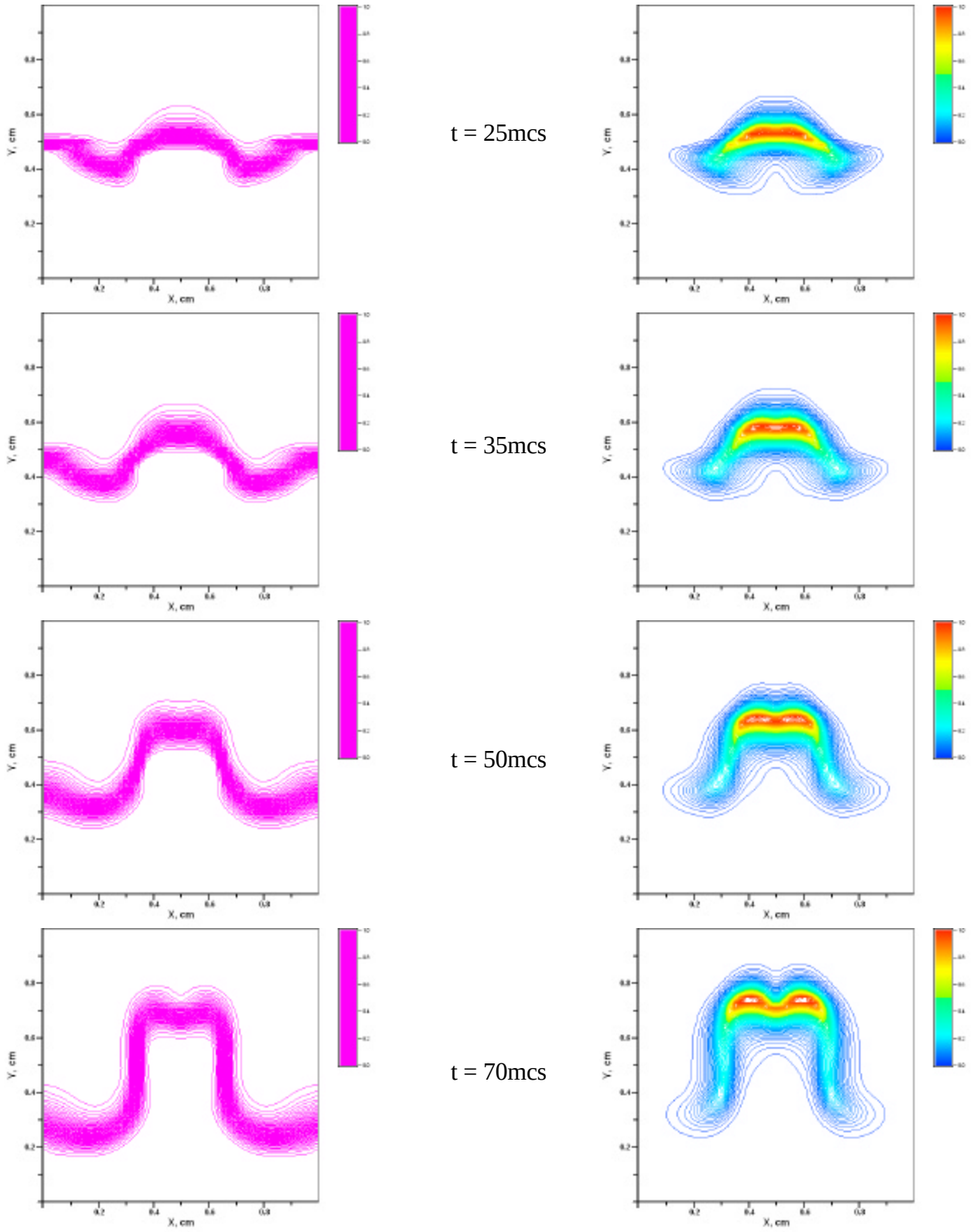

Fig.1a. The mass fractions of hydrogen and water(left) and temperature(right) for Case 1 (no chemistry, cont.).

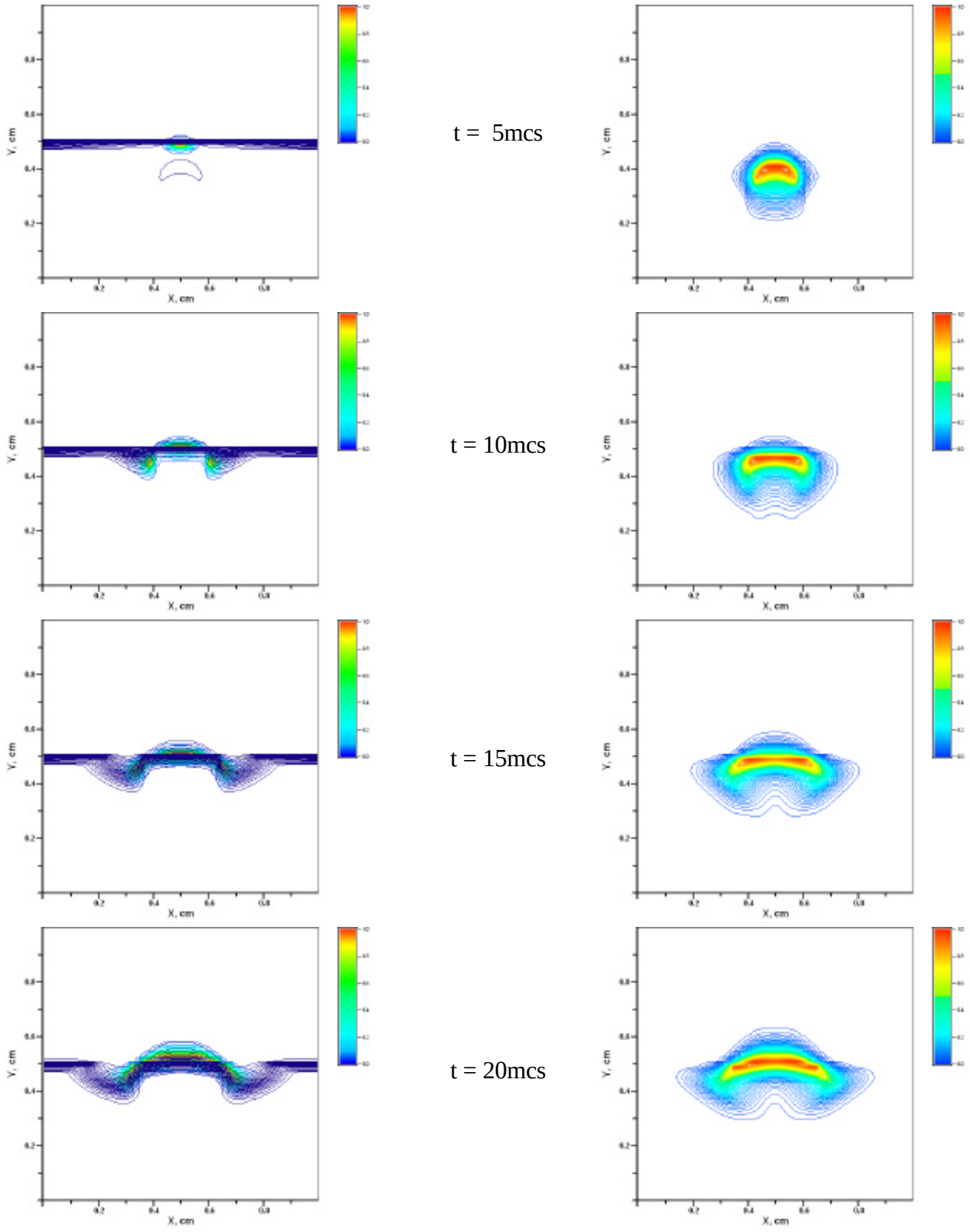

Fig.2. The mass fractions of hydrogen and water(left) and temperature(right) for Case 1.

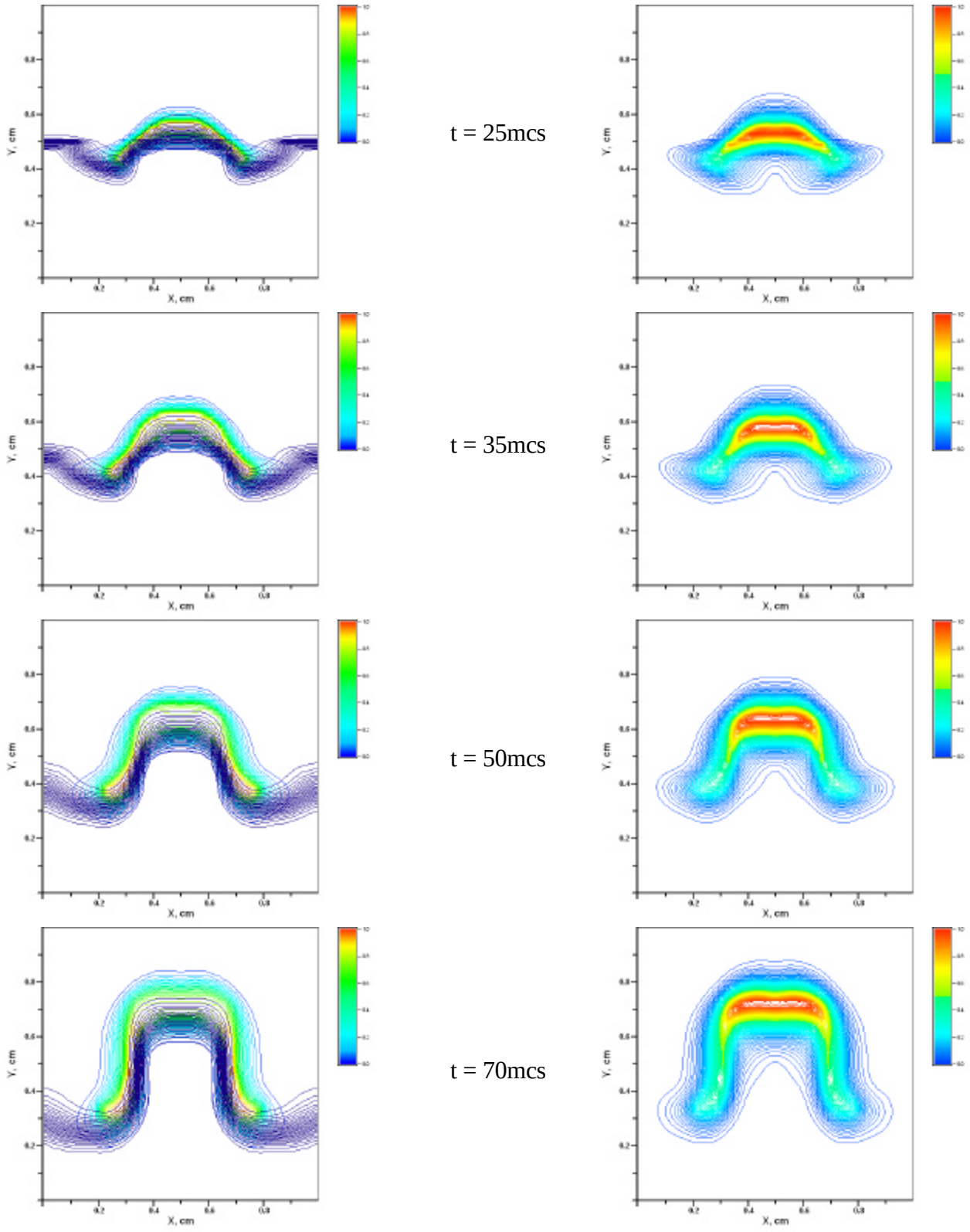

Fig.2a. The mass fractions of hydrogen and water(left) and temperature(right) for Case 1 (cont.).

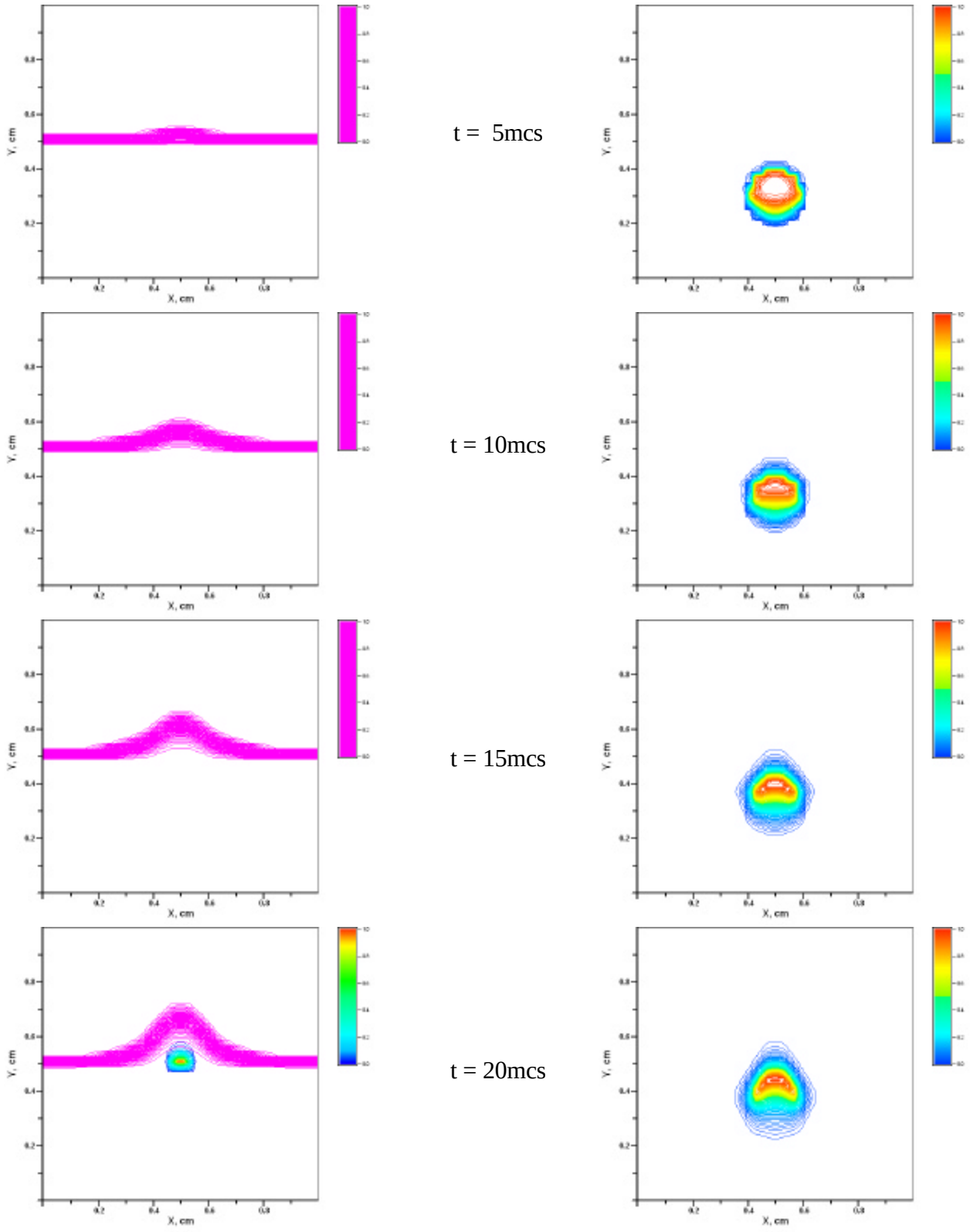

Fig.3. The mass fractions of hydrogen and water(left) and temperature(right) for Case 2.

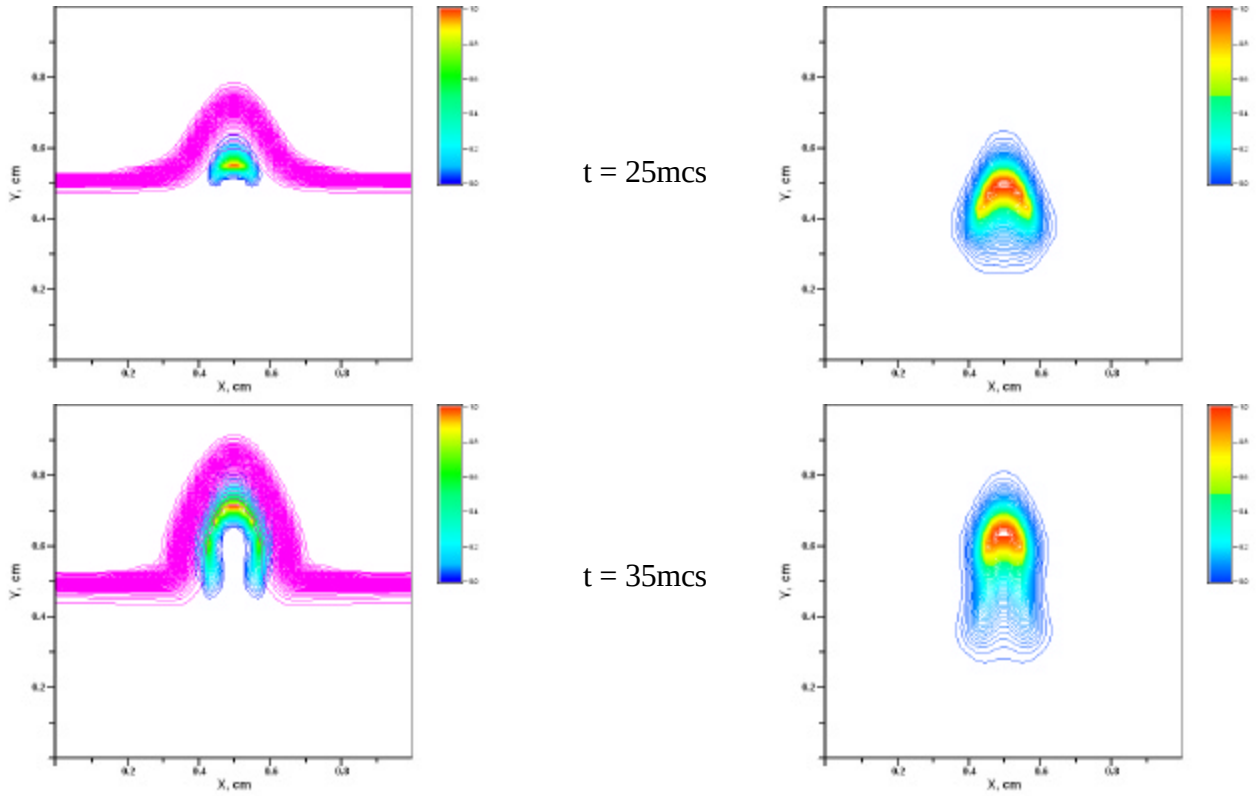

Fig.3a. The mass fractions of hydrogen and water(left) and temperature(right) for Case 2 (cont.).

IV-2. Post-Discharge Reacting Volume Evolution

In the previous Section the numerical study of the enhancement of mixing/combustion in hydrogen-air mixture by the MHD-driven arc column has been carried out. In these experiments both electric current and magnetic field were permanently maintained during the computations.

In order to understand what is an *ignition* capability of such an MHD driving mechanism the next step study has been undertaken to observe the evolution of the reacting volume after the current and/or magnetic field switches off. The problem configuration is basically the same as it was used in the previous Section. The following two problems were considered.

Case 1: as well as in the previous work the arc initiates in hydrogen and enters into the air due to electromagnetic force. 25 microseconds after the arc generation the magnetic field is switched off, while the electric current remains.

Case 2: 25 microseconds after the arc generation both electric current and magnetic field are switched off.

The previous formulation, i.e. current + magnetic field on, will be denoted as Case 0. In all three cases the computations were performed for 45mks (70mks after initiation). The two-dimensional fields of temperature and water concentration are presented in Fig.4. Initial state corresponding to t=25mks is shown in Fig.4a. In Fig.4b the fields at t=70mks are presented for Case 0.

Fig.4c corresponds to the Case 1 and the same time t=70mks. Fig.1d shows the fields corresponding to Case 2 at t=70mks. In all pictures the temperature ranges from T_{min}=300K to T_{max}=4300K, ΔT=50K. The water mole fraction varies from C_{min}=0 to C_{max}=0.24, ΔC=0.005.

In the Case 0 the largest combustion zone is observed. The arc motion increases mixing which provides more intensive combustion. In the Case 1 the arc slows down and mixing is mainly due to diffusion of species. In the Case 2 the arc kinematics is nearly same as in Case 1. The size of the arc is slightly larger in Case 1 than in Case 0 because of Joule heating. Maximum temperature is nearly same as in Case 0, 4000K. In Case 2 the maximum temperature is about 1700K. However this large difference doesn't play any role, since combustion initiates at rather moderate temperatures. One can say that in no current case the temperature is maintained only due to combustion. The total production of water, which is considered as the combustion efficiency, is approximately equal for both no-interaction cases. This is well seen from Fig.5, where the total water production is given against the time. The Curve 1 on the plot corresponds to Case 0, Curve 2 corresponds to Case 1, and Curve 3 corresponds to Case 2. Maximum production is observed for Case 0 because of more developed interface surface due to arc motion. Another feature of combustion process can be seen from Fig.3, where the total enthalpy of the fluid volume vs. time is shown for the same cases as

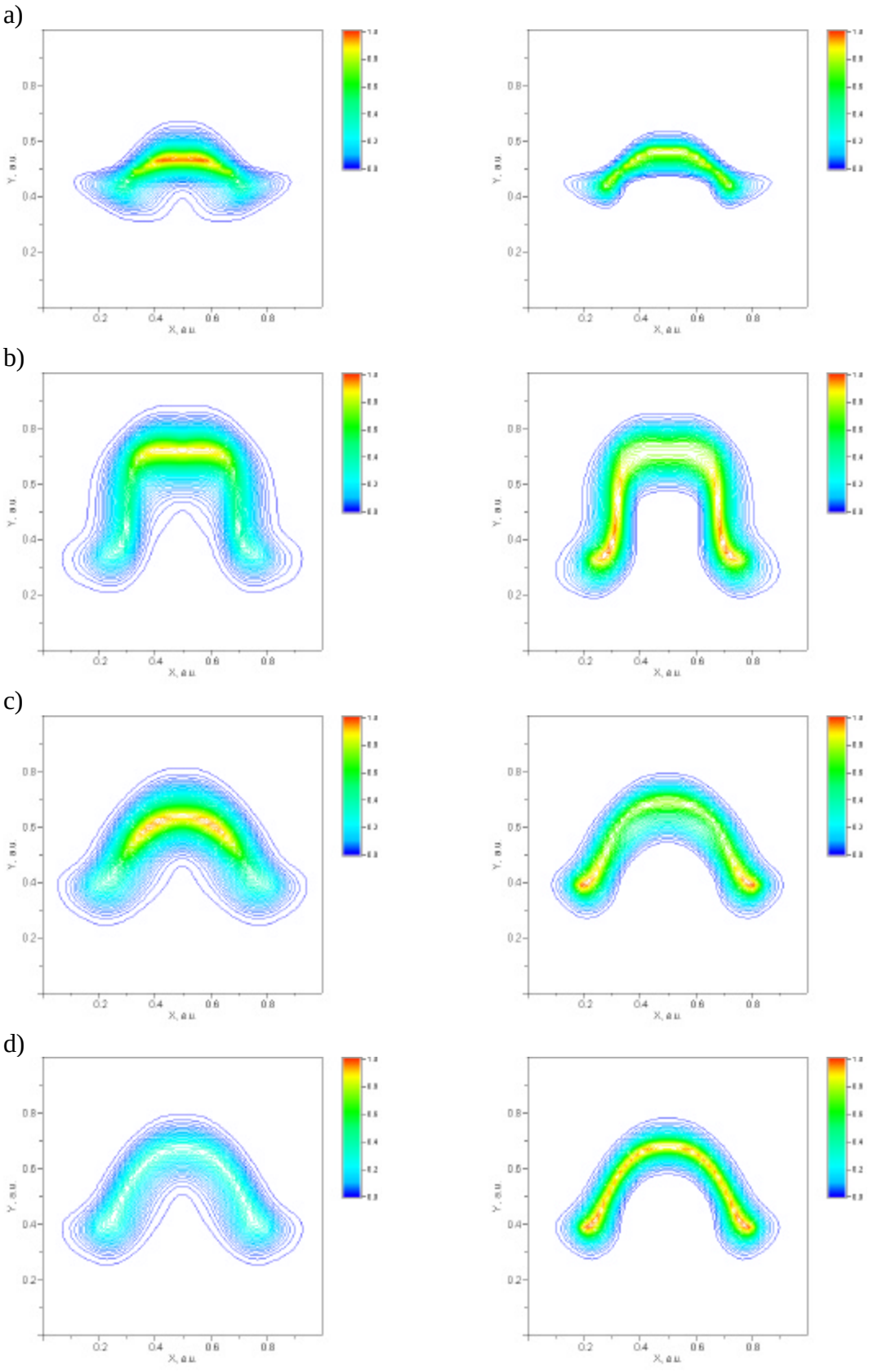

Fig.4. Temperature(left) and water concentration(right) for initial state(a); Case 0(b), Case1, Case 2; *t*=70mks

those in Fig.5. While energy input in Case 1 increases in time, the water production, as combustion efficiency sensor, is not effected by this circumstance. The maximum production rates are observed at rather moderate temperatures. At high temperatures, say above 2500K, dissociation processes prevail.

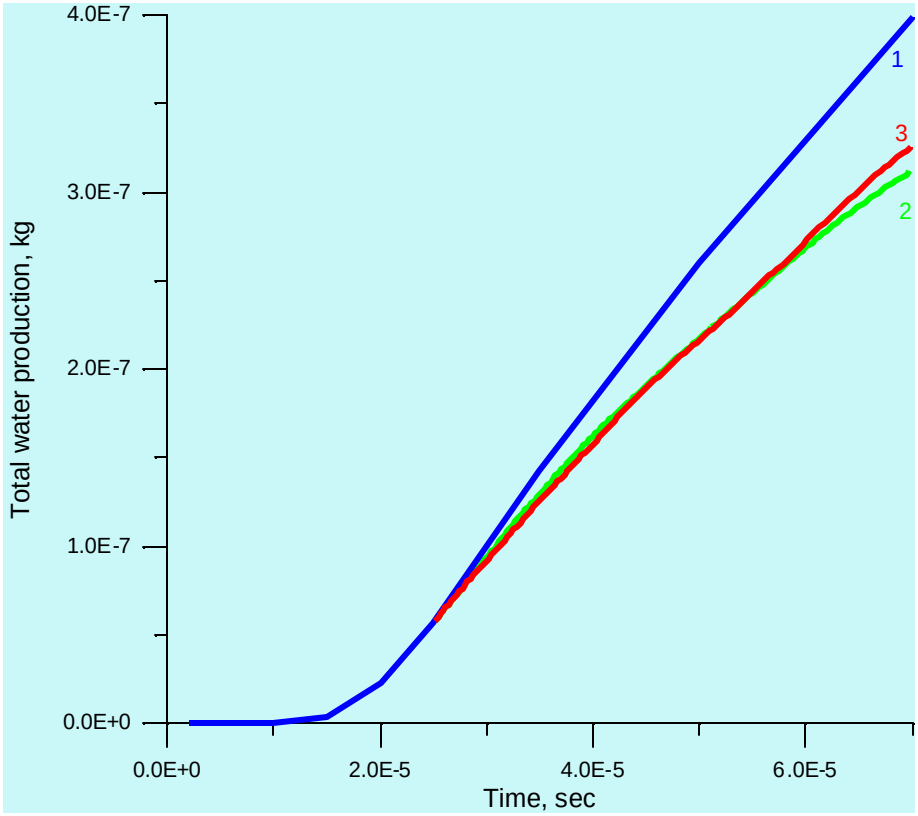

Fig.5. Total water production for Case 0(Curve 1), Case 1(Curve 2) and Case 2(Curve 3).

Thus, one could conclude that MHD-interaction does effect on mixing and combustion. At first turn, this is due to the motion of the arc. Electromagnetic forces increase the total vorticity in fluid and make mixing more intensive. The heat input seems to play the role of starter: mixing of components should be performed at even moderate temperatures (above 1200K); then self-sustained combustion could start. Initial mixing and igniting of mixture can be effectively performed with MHD-interactions.

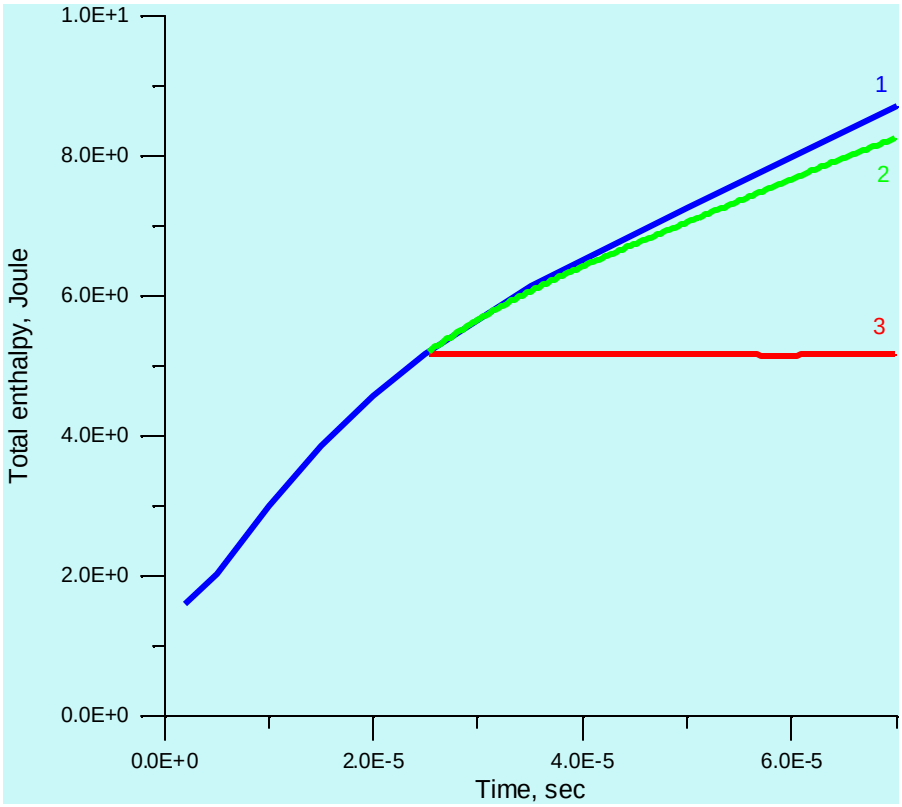

Fig.6. Total enthalpy for Case 0 (Curve 1), Case 1 (Curve 2) and Case 2 (Curve 3).

IV-3. Numerical prediction of arc-driven mixing and combustion under experimental conditions

The previous work has been intended to study the capabilities of the arc discharge driven by the magnetic field to enhance the mixing and combustion in the non-premixed mixtures. The simplified problem has been considered, in which hydrogen (fuel) and air (oxidizer) were originally separated. Mixing and combustion were stimulated by the electric arc moved by the applied magnetic field across the fuel-oxidizer interface. It was numerically shown that the motion of the arc increases the contact surface while the high temperature within arc provides ignition and combustion around the interface. It was found that combustion occurs during rather long time after switching off the electric current.

These results stimulated us to perform the next series of numerical experiments. The goal is to study combustion in non-premixed fuel-oxidizer jets. The numerical formulation is assumed to be close the conditions of small-facility experiments. Such facility is now being designed. The interaction of two flat jets is considered. The electric arc normal to the flow is generated by the electrode system so that the arc current is constant. Magnetic field created by the coil is directed along the flow. Such configuration enforces the arc to move across the jet interface. In numerical predictions we shall consider the following formulation. Let two jets flow in X-direction. The jet of hydrogen is initially located in the lower half-plane, and the jet of air occupies the upper half-plane. The size of the domain in X-direction is taken to be 4cm, the size of each jet in Y-direction is taken to be 0.5 cm. The flat velocity profiles are assumed for simplicity at the inlet station. On the rest of the domain boundary the outflow conditions are specified. Initial velocity field corresponds to the inlet conditions overall the domain. Z-directed electric arc of 2mm in diameter is initiated at 3 mm downstream the inlet station and 1 mm below the jet interface. Initial temperature within the arc was taken 4000K, which is not so important as found from previous calculations. Duration of the arc discharge was taken 20 microseconds, and constant total current 10A was set. The constant X-directed magnetic field of 1 Teslas was assumed. The following flow parameters were used: pressure - 1bar, temperature - 300K for both jets. Two sets of jet velocities were considered.

Case 1: both air and hydrogen inlet velocities were set to 100 m/s;

Case 2: air inlet velocity equals to 100 m/s and hydrogen inlet velocity equals to 200m/s.

The problem formulated above was solved by the control-volume method. Exact Riemann solver was used to evaluate convective fluxes at the cell boundaries. Diffusive fluxes were estimated by the method similar to central-difference scheme on the orthogonal grids. Four-stage Runge-Kutta time-stepping was applied with constant CFL-number equal to 2. The chemical source-terms (rates of species production) were evaluated in implicit manner using special kinetic solver. The computational grid consisted of 200 cells in flow direction and 100 cells in transversal one.

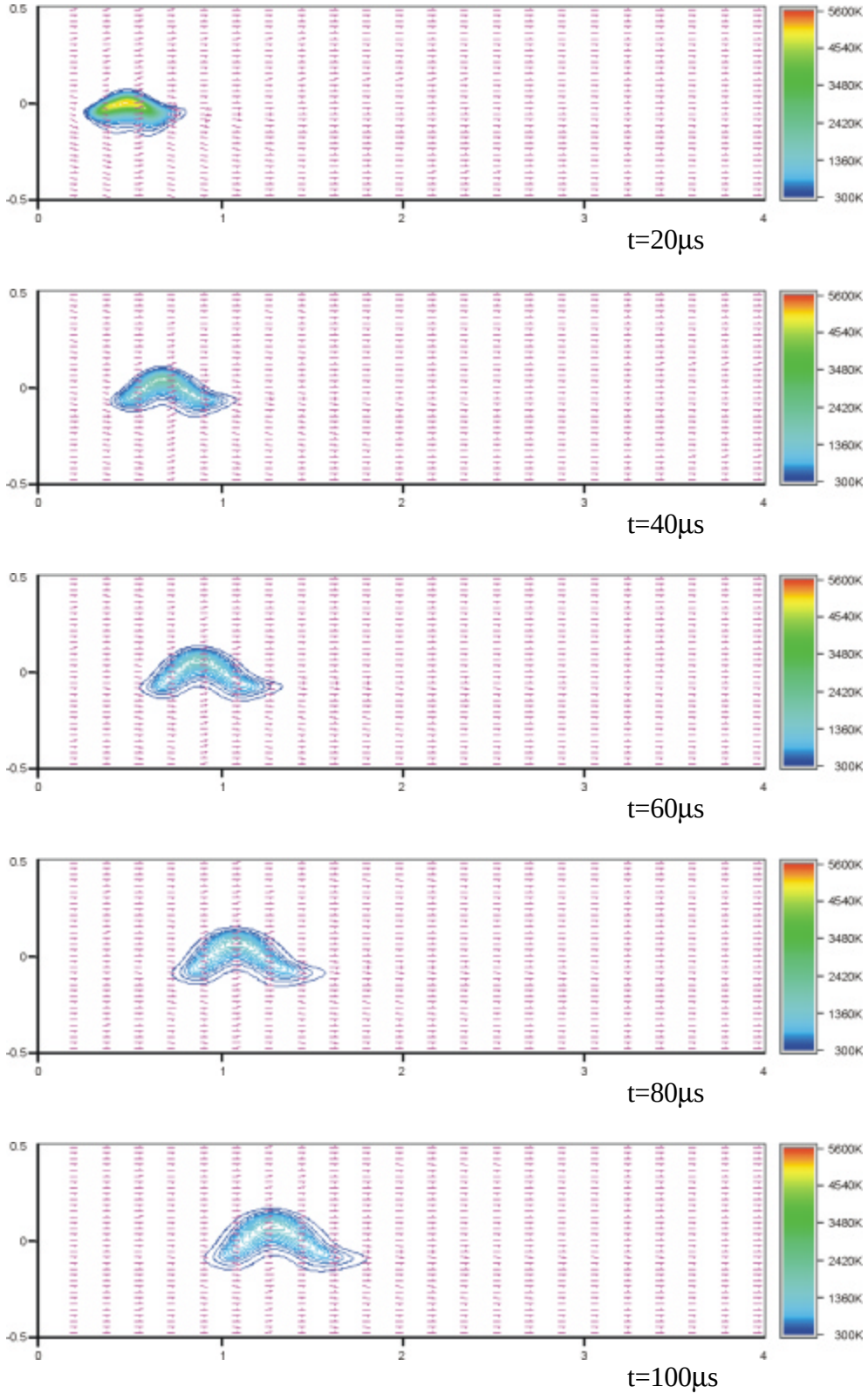

Figs 7. Temperature and velocity vectors, Case 1.

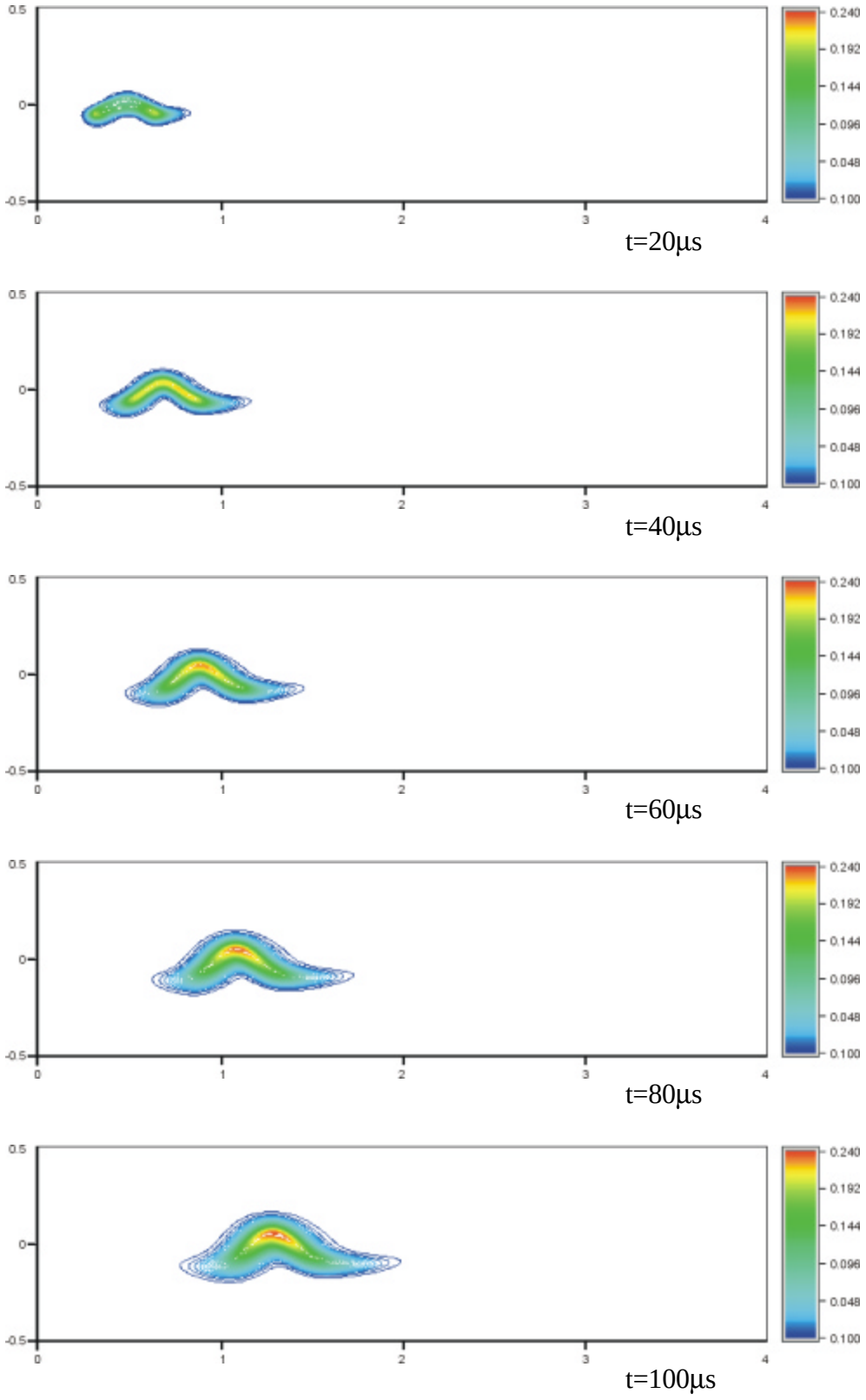

Figs 8. Water mass fraction distributions, Case 1.

The main features of flow can be seen from Fig. 7 and Fig. 8 corresponded to Cases 1 and 2, respectively. Fig.7 shows temperature and velocity fields for Case 1 at different time moments.

Fig.8 shows the distribution of water mass-fraction at the same time moments. Fig.9 and Fig.10 represent the analogous distributions for Case 2. The time values are given in the pictures.

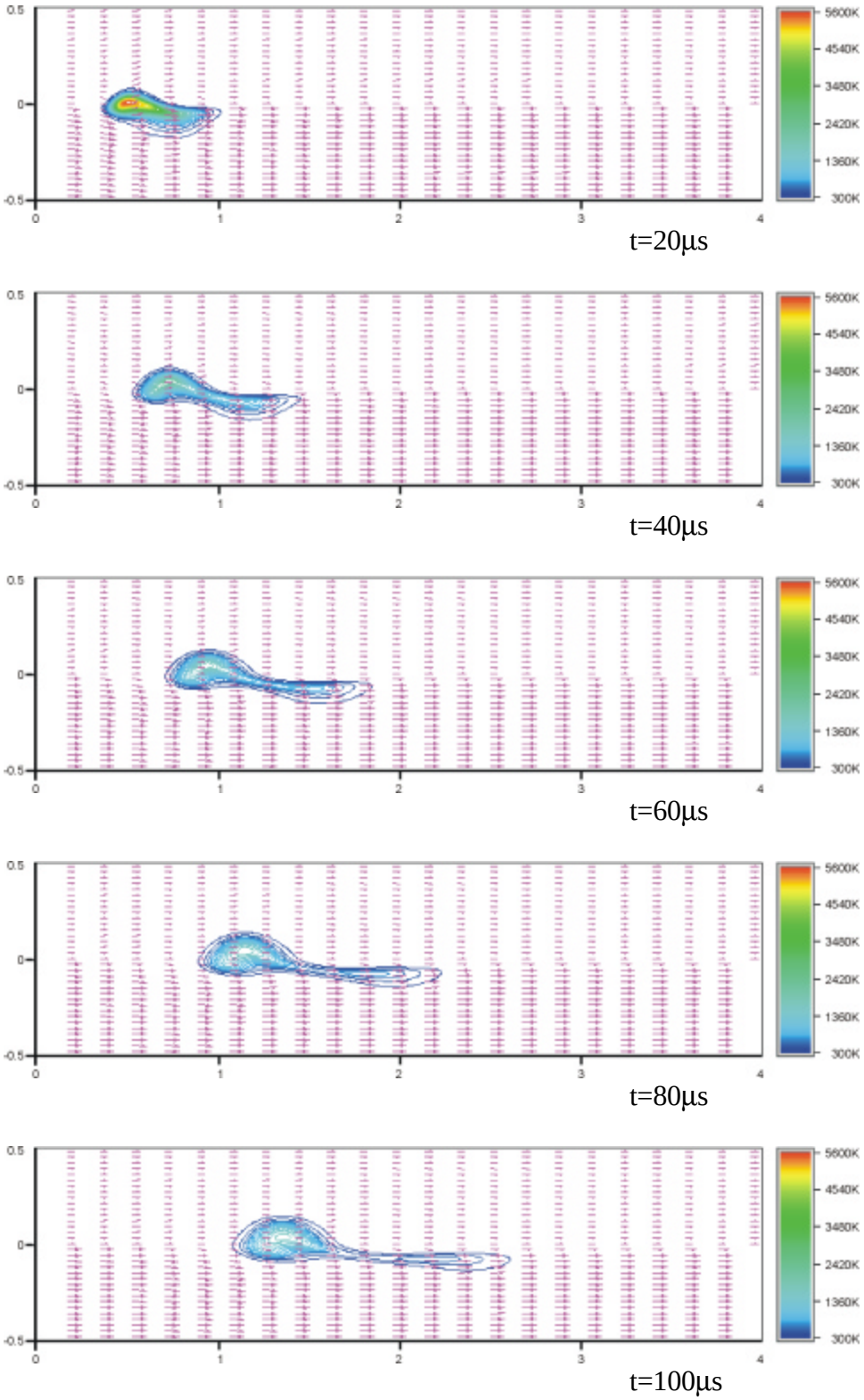

Figs. 9. Temperature and velocity vectors, Case 2.

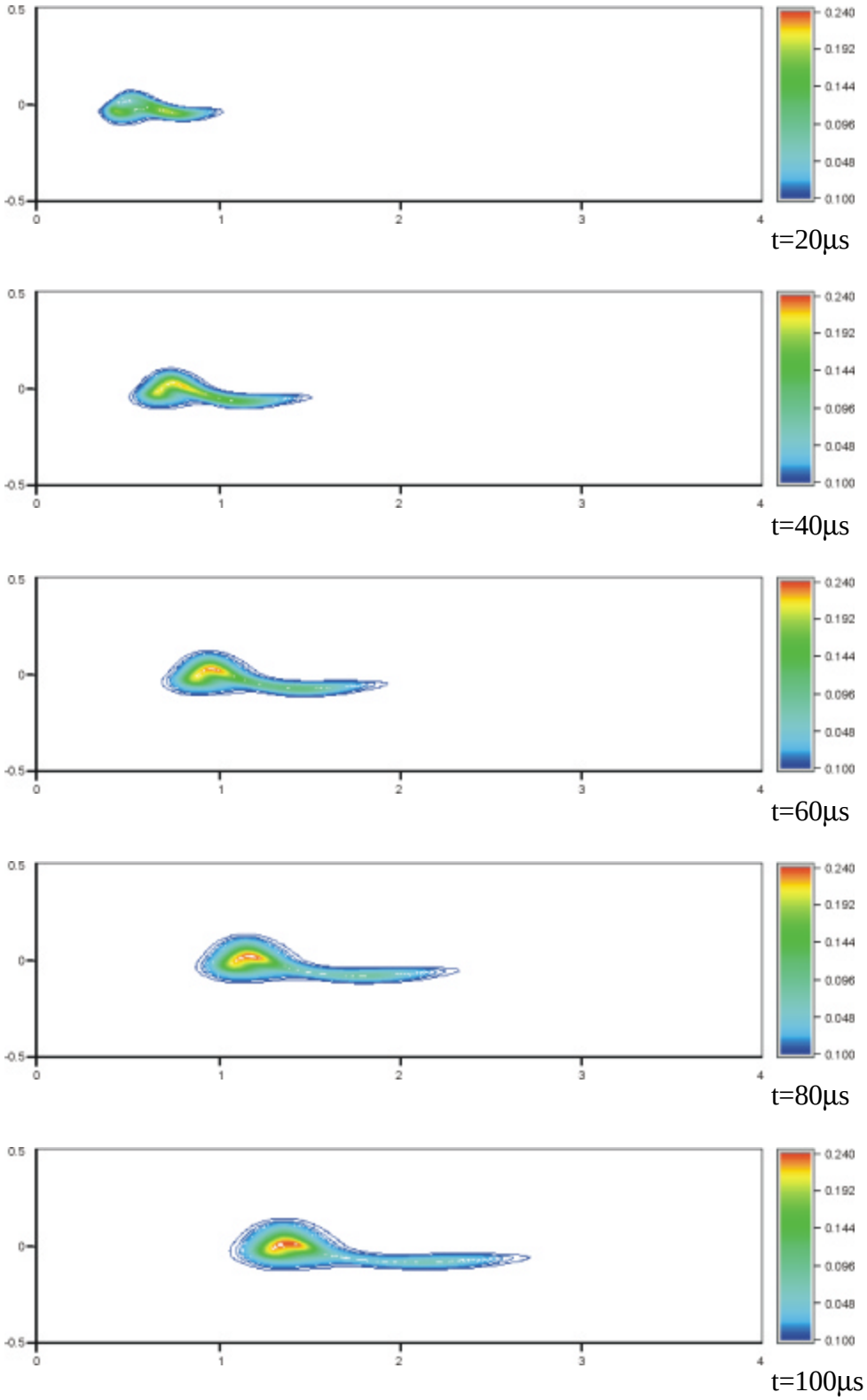

Fig.10. Water mass fraction distributions, Case 2.

The characteristic feature of the flows under consideration is that originally small arc creates the spot with well-developed reaction zone, in which combustion can support the existence of the spot during a long time compared to the arc life-time.

The formulations considered above were used as the first-stage predictions to parameters of the small-scale facility being designed. In a future coupled experimental work and numerical analysis is hoped to give more knowledge about the topics of interest.

IV-4. The Reacting Volume and Vorticity Evolution due to the Body-Force

In order to prove the reacting volume concept used in this work for all problem formulations let us consider the quantitative description of the process in question.

The reacting volume value can be define as

$$V_r = \int_{V_o} \sum_i X_{i,O} \cdot \sum_j X_{j,F} dV \; ;$$

where $X_{i,O}$ and $X_{j,F}$ are the mole fraction of i-th oxygen-containing species and the mole fraction of j-th fuel-containing species. The summing should be made on all species in the mixture. In principle, such a definition of the reacting volume value could be normalized with a limiting value corresponding to uniform mixture. However, the constant factor omitted in the expression written above is non-important in the further analysis. One can see also that at the initial state when two uniform volumes of fuel and oxidizer are put into contact the reacting volume V_r defined here is equal to zero. It is also clear that the reacting volume is a measure of "combustion" reactions rate between fuel- and oxygen-containing molecules.

Two others parameters will be used further in this section.

The first one is a species production

$$Q_i = \int_{V_o} C_i dV \; ;$$

where C_i is the weight fraction of i-th species. In this particular case the two product species will be used: H_2O and OH, to characterize the overall combustion productivity. Again, non-normalized values are acceptable for the particular purposes of the analysis.

The characteristics of the flow field disturbances created by a body-force $\mathbf{j}\times\mathbf{B}$ is given by the integral vorticity defined as

$$\Omega = \int_{V_o} |\mathbf{rotv}| dV.$$

This parameter represents the integral vorticity of the flow field in the domain that is responsible for the enhancement of the kinematics mixing due to the stretching of a fluid volume of the media. The mechanism of this process is described in details in our preceding work [1].

As an example of MHD-assisted mixing and combustion the computational domain and the initial and boundary conditions similar to those considered in the Sub-Sections IV-1 and IV-2 are utilized.

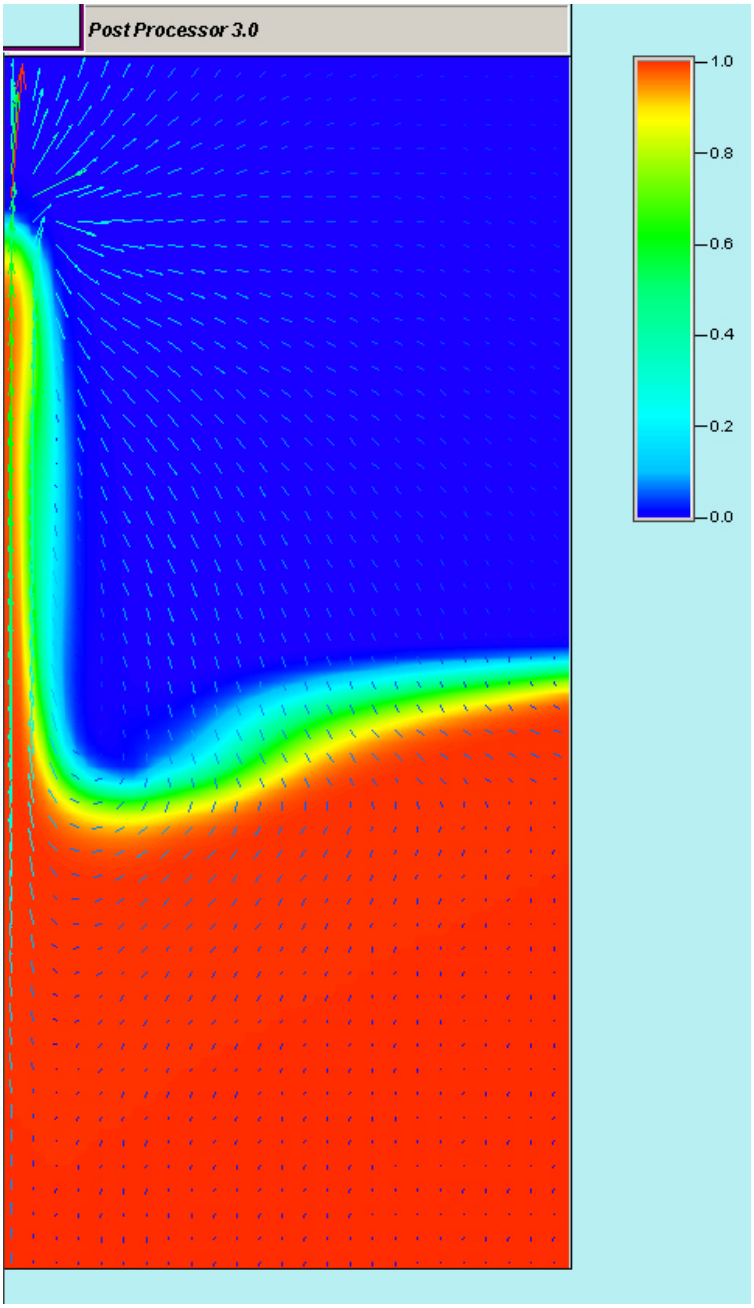

Fig. 11. Flow Field and Fuel Mole Fraction Distribution at t = 70 mks

In the Fig.11 the flow field structure (the right half of the domain is shown because of the symmetry) and the fuel mole fraction (hydrogen) are presented at the time moment t=70μsec. It is

clear from the picture that the reacting volume represented here by the colored area between the red (100% fuel) and blue (0% fuel) is increasing significantly due to the vortex flow field created by the body force. In Fig.12 the corresponding value of the reacting volume value V_r defined above is shown. The irregular behavior at the initial stage is caused probably by the starting shock wave created by the heat release in the arc and the following the mass loss through the domain border. After that the practically linear growth of the reacting volume is observed. It is interesting that total mass production of the combustion ignited by the heating is also practically linear in respect to time. One can conclude that the mixing process (the formation of the reacting volume) is of primary importance for the combustion efficiency. At the same time it should be noted the H_2O production reveals a slight accelerating due to probably cooling at the periphery of the reacting area providing the conversion of OH to H_2O.

The information supporting this conclusion is presented in Fig.13 where the vorticity generation is plotted. The irregular interval at the beginning of mixing and combustion induced by MHD body force is even more clearly seen from this plot.

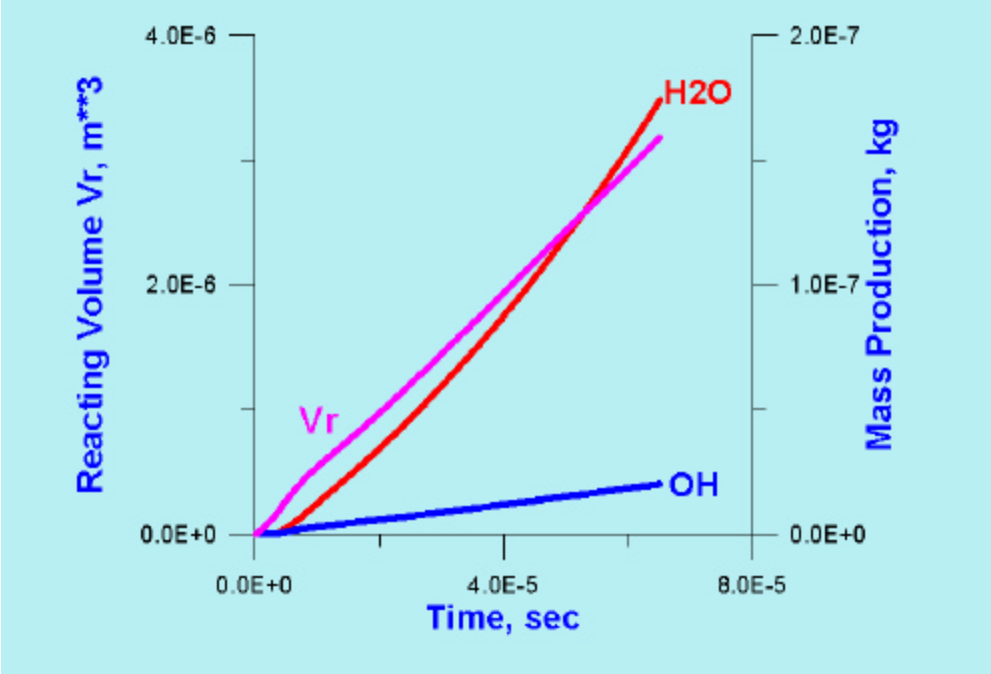

Fig. 12. Reacting Volume and Mass production of H_2O and OH vs time

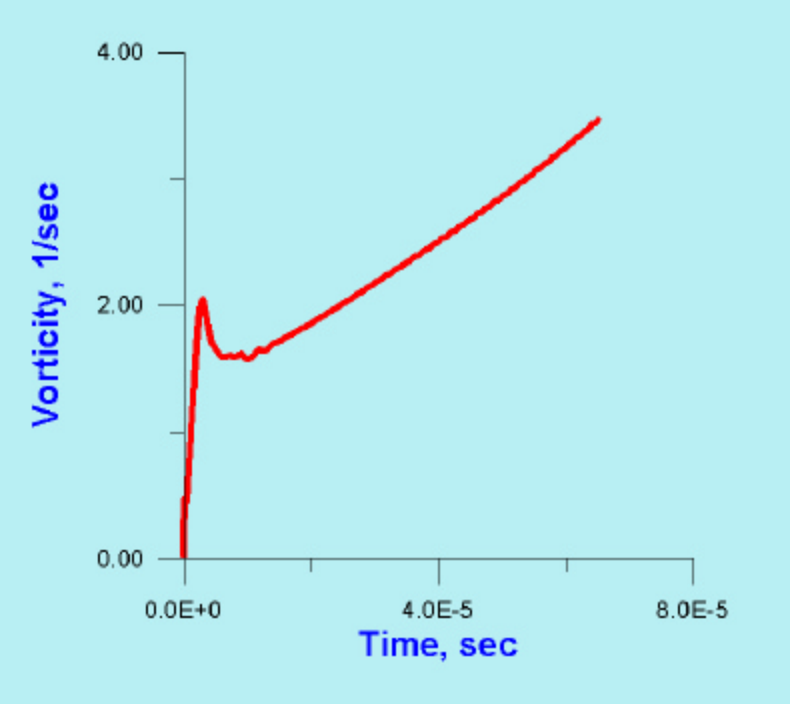

Fig. 13. Vorticity Evolution in Time

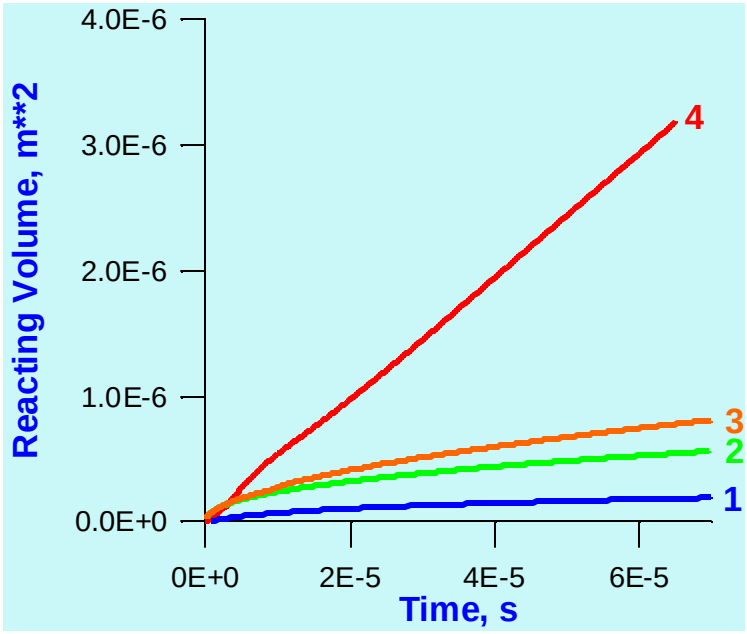

Fig.14. Reacting volume vs. time. Curve 1: diffusion only, constant temperature 300K; Curve 2: diffusion only, hydrogen temperature 3000K; Curve 3: diffusion and combustion, hydrogen temperature 300K; Curve 4: MHD-assisted combustion.

To light up the reacting volume concept let us consider the simple test. The same initial fuel/oxidizer state is considered, i.e. hydrogen is “specified” in the bottom part of the domain and the oxidizer (oxygen) is specified in the top part. The system is maintained at the room temperature. The reacting volume in this case is the potential zone where the combustion could take place if it were ignited. The reacting volume is exactly the diffusion layer which is small and grows in time as square root. The development of no-combustion reacting volume is presented in Fig.14 by the Curve 1. The temperature dependence of the no-combustion reacting volume is demonstrated by the Curve 2 in the same plot. This curve stands for the initial temperature of hydrogen 3000K. The larger reacting volume as compared to the previous case is due to enhanced diffusion coefficients because of higher initial temperature. The Curve 3 in Fig.14 corresponds to the initial state of the previous case, but with the combustion allowed. Slight increase of the reacting volume id thought to be due to expansion because of heat release. For comparison, the reacting volume corresponding to the MHD-assisted combustion from the previous graph is also shown as Curve 4. The difference between MHD-assisted combustion and non-MHD one is evident.

V. EXPERIMENTAL FACILITY PRELIMINARY DESIGN

V-1. Experimental Scheme Development

The experimental validation of the proposed MHD assisted mixing mechanism will be a subject of the future work of the 2nd year activity of the Project. At this stage a preliminary analysis of the possible approaches is undertaken.

The schematic diagram oft he proposed experimental setup is presented in Fig.11.

The main components are as following:

1. High pressure vessels for working gas storage;
2. The nozzles for formation of two co-flow streams of the gas to be mixed;
3. Electrodes system to provide pulse electrical discharge in the flow;
4. Pulse magnetic system to create magnetic field in proper direction in the mixing volume;
5. Power supply systems of electrical discharge and the magnetic system;
6. Diagnostics/visualization equipment;
7. Ventilation

It is proposed to use at the first stage two contrast colored gases such an air and smoked gas. Another possibility acceptable in a case of utilization of the Schlieren technique could be a mixing experiment with two streams with different temperature (density).

The proposed scheme of the experiment consists of the several steps:

1. The initialization of the co-flow free jets in the test volume;
2. The initialization of the pulse discharge across the streams parallel to the interface between two gases;
3. The synchronized induced magnetic field should be oriented perpendicular to the main discharge current, and correspondingly parallel to the interface;
4. The visualization system should record the effect of the j*B pondermotive force acting in the vicinity of the interface.

At the next stage the ignition and combustion process affected by the pondermotive force and concentrated heat release due to Joule dissipation will be studied as well.

The experimental parameters are estimated with utilization of the results of the theoretical analysis and numerical simulation.

As it was already mentioned in the previous Interim report the typical value of the current should be around 10 Amps, and the magnetic induction is about 2-3T. These parameters provide the current channel displacement in several millimeters resulting in penetration of heated portion of one component to another co-flow stream during the observation time. The latter is defined by the velocity of the flow and the size of observed area.

The discharge current will be provided by high voltage (30-50 kV) power supply – the standard high voltage transformer with rectifier BT-140. This transformer will be used to charge high voltage capacitor ? ? ? -12 of 12 mkF through two load resistors ???-20 of 4.3 MOhm each. This could provide a discharge current pulse about 100Amps, at voltage 30 kV and duration about 1 msec. The estimated interelectrode gap is about 3 cm.

The magnetic system will consists of the coil of 5 turns with 6 cm in diameter. The coil current of 10 kAmps will result in the 1T magnetic induction in the test volume. The power supply of such a magnet will be solved with a standard high voltage power supply of BT-20 that will charge a capacitor bank of 20 K41?-7 units with total capacity of 2 mF at the voltage 5 kV. In order to provide the pulse duration more than 1 msec (that is a synchronization condition with discharge current duration) the total inductance should be not less than 12 mkH. Thus, the inductance of system can be fitted with the coil turn number used. It should be noted that increasing the number of coil turn results in increasing of magnetic induction that is very desirable for the final purposes of the experiment.

The synchronization of the test consequence will be provided with the CAMAC system available at the site.

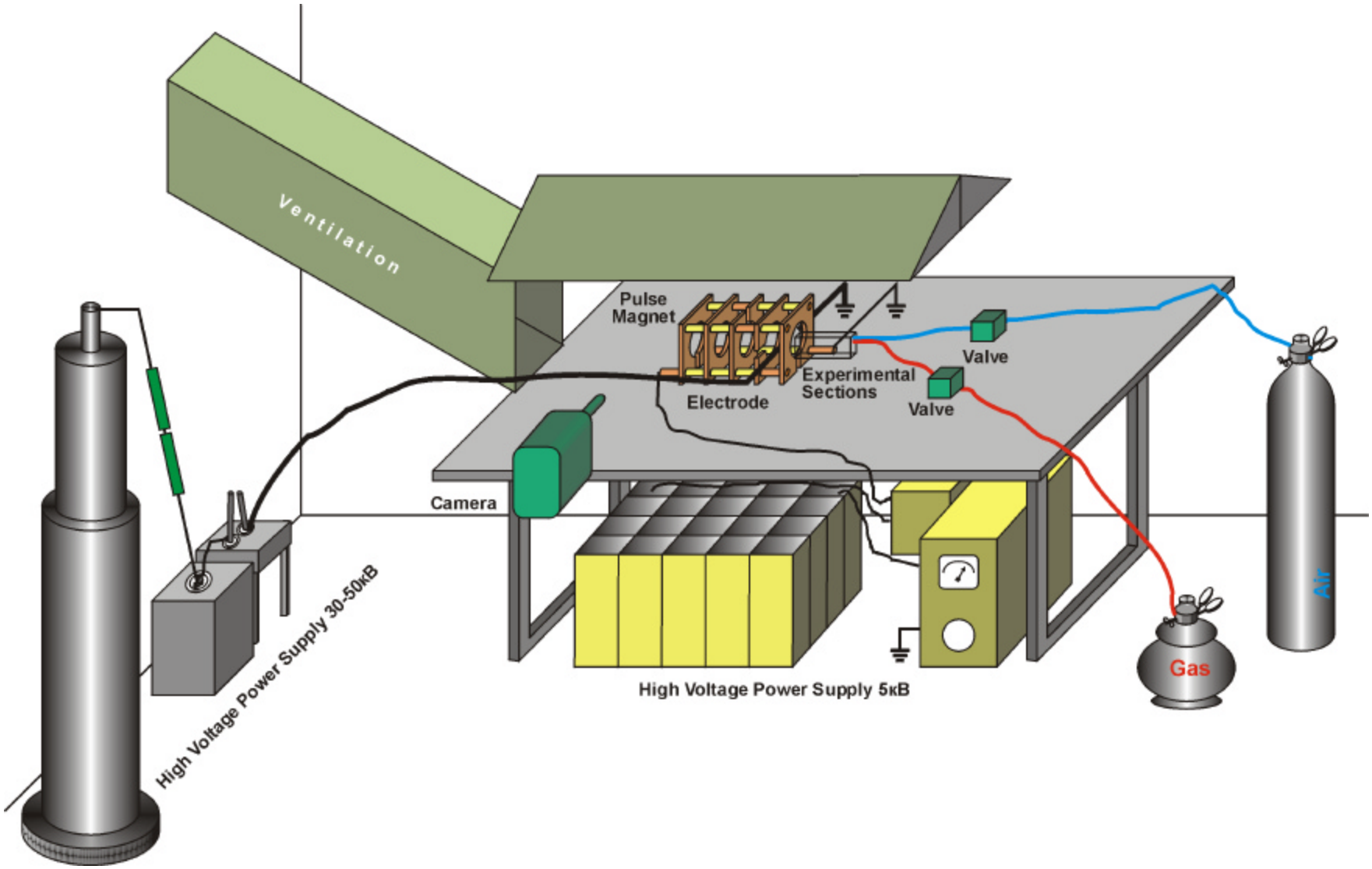

Fig.4. Layout of experimental rig on MHD assisted mixing

V-2. Experimental rig assemblage.

The schematic diagram of preliminary proposed experimental facility presented and briefly discussed in the previous Sub-Section is used now in preparation of the experimental study of the MHD driven mixing and, the second, stage ignition and combustion.. At the present time the experimental facility is being to be assemblage and tuned. The first stage is aimed to create the simplest working version of the experiments to check the different options of the experimental program and arrangement.

In Photos 3.1 through 3.3 the current view of the assemblage is presented.

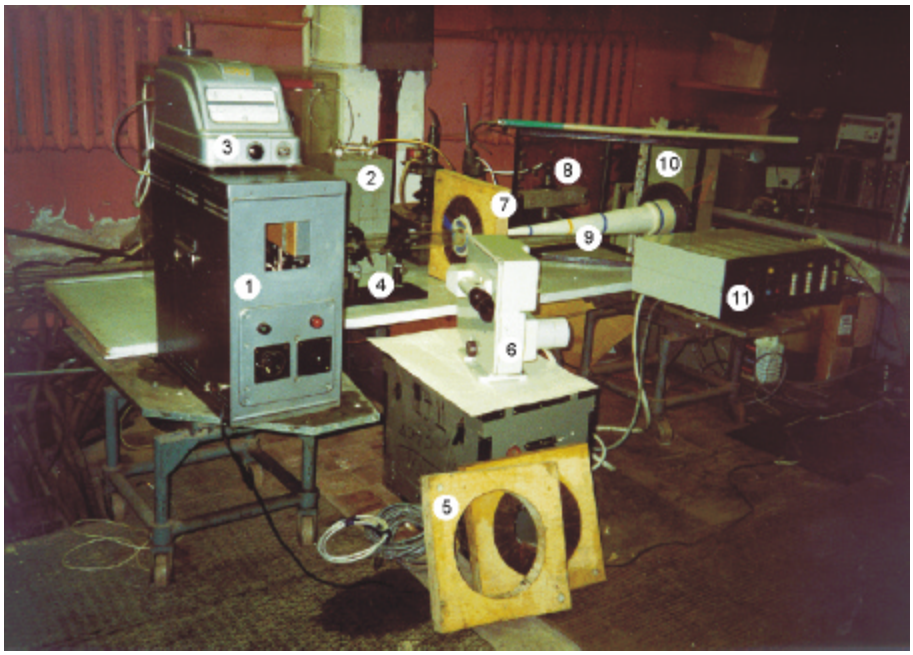

Fig.3.1 The Experimental Assemblage of the MHD Assisted Mixing Study

The main components are as follows. 1 – High voltage supply BC20 for the voltage 0–20 kV; 2 – capacitor of 100mkF (two pieces0; 3 – high voltage voltmeter; 4 – quartz tube of exhausting system; 5 – example of the magnetic coil strength elements; 6 – the fast camera ????-16 of 5000fr-sec maximal ñ 7 – magnetic system installed; 8 - mercury switcher ???-6; 9 – converging nozzle; 10 – ventilator; 11 – the fast camera controller.

Fig.3.2. The side view of the experimental set-up

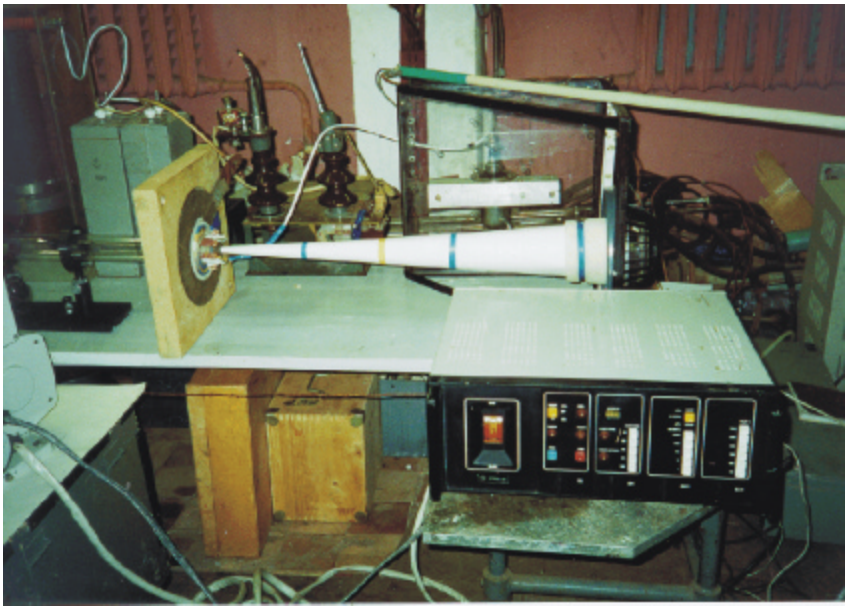

Fig.3.3 The nozzle and the magnetic coil view in assemblage

The components of the experimental set-up are tested now.

CONCLUSION

The new concept of MHD driven Advanced mixing of gaseous fuel-oxidant system in a high-speed combustor is formulated.

The background of such a concept consists of the earlier developed model of kinematics mixing in vortex turbulent flows.

The vortex nature of the Lorentz body force resulting from perpendicular vectors of electrical current and externally applied magnetic filed provides the flow vorticity intensification.

The enhancement of the mixing under such conditions is characterized by an exponential growth of the contact surface square in a turbulent flow.

The second mechanism – molecular diffusion is responsible for the creating the flammable mixture in a physically small volume.

These two mixing mechanisms are combined to formulate the concept of reacting volume – the volume where the combustion is only possible.

Besides of the qualitative physical model the proper numerical model has been developed to study the process on the microscopic scale.

This model includes the treatment of chemical reacting flows on the base of full Navier-Stockes approach, chemical kinetics model, and MHD effects model.

Preliminary results confirm the basic physical ideas. The combustion in co-flow streams can be effectively initiated and controlled by the manipulation of the electrical parameters: strength of external magnetic field and electrical discharge current.

The dramatic growth of the reacting volume and, hence, the combustion performance in the presence of MHD interaction was clearly demonstrated.

The preliminary sketch of the future laboratory scale experiment is presented as well.

The parametric study of the proposed concept as applied to the conditions typical for the practical situation in a scramjet/ ramjet will be completed in a related project supported by ISTC in 2000/2001.

Acknowledgement

The authors are gratefully acknowledged to EOARD and personally to Dr.C.Raffoul for financial and moral support during the project.

References

1. V.A.Bityurin,Advanced Mixing of Fuel/Oxidant System in High Speed Gaseous Flows. Stage 1. Final report on EOARD Contract SPC 99-4093, 2000
2. Hirschfelder J.O., Curtiss C.F. and Bird R.B. Molecular Theory of Gasses and Liqids, John Willy and Sons, New York, 1954.
3. Anfimov N.A. Liminar Boundary Layer in Multi-Component Gas Mixture, Izv.USSR Acad. Sci., Mechanics and Mashinary, 1962, No.1, pp.25-31 (in Russian).
4. Gordeev O.A., Kalinin A.P., Komov A.L., et.al. Obsory po teplofisichekim svoistvam veskhestv, No.5 (55). M: USSR Acad. Sci., IVTAN, 1985.
5. Gerasimov G.Ya., Kalinin A.P., Lusternik V.E., at.al. Obsory po teplofisichekim svoistvam veskhestv, No.5 (67). M: USSR Acad. Sci., IVTAN, 1987 (in Russian).
6. Freeman and Oliver, High Temperature Thermodynamics and Transport Properties in the Models of Planetary atmospheres created by CO-N, Rocket Techniques and Space (RTK), 1970, No.9, pp.183-191 (in Russian).
7. Reed P., Sherwood T. and Prawsnitz J. Properties of Gases and Liquids, L: Chimia (Chemistry), 1971 (in Russian).
8. Afonina N.E., Gromov V.A. Finite Volume Method for Numerical Calculation of the Flow Over Blunt Body with Thermo-Chemical destribution of Heat-Protected System. In: Physical and Gasdynamic Phenomena in Supersonic Flows Over Bodies. Edit. By N.N.Pilyugin, Inst. Of Mechanics of MSU, Moscow State University, Moscow, 1998 (in Russian).
9. M.Capitelli, C.Gorse, S.Longo, and D.Giordano, Transport Properties for High Temperature Air Species, AIAA Paper 98-2936, 1998.

Nomenclature

$\mathbf{J}$	– electric current density
$\mathbf{B}$	– magnetic induction vector
L, l	– characteristic lengths
t	– time, characteristic time
$\mathbf{U}$	– conservative-variable vector consisting of fluid density, momentum, total energy and species densities
$\mathbf{F}$, $\mathbf{G}$	– inviscid flux-vectors in x- and y-directions, respectively
$\mathbf{F}_v$, $\mathbf{G}_v$	– viscous flux-vector in x- and y-directions
$\mathbf{S}$	– source-term vector
ρ	– fluid density
$\mathbf{v}=(v_x,v_y)$	– fluid velocity
E	– total specific energy
Y_i	– species mass-fractions
X_i	– species mole-fractions
P	– thermodynamic pressure
τ_{ij}	– viscous stress-tensor components
$\mathbf{J}_i=(J_{xi};J_{yi})$	– mass diffusion flux of species i
$\mathbf{e}=(e_x,e_y)$	– energy flux due to heat conductance, viscous dissipation and multi-component diffusion
μ	– molecular viscosity coefficient
λ	– molecular heat conductivity coefficient
T	– temperature
h_i	– specific enthalpy of species i
$h_{i,f}$	– formation enthalpy of species i
D_{im}	– effective mass-diffusion coefficient of species i
N	– number of species
D_{ij}	– binary diffusion coefficients
W_i, M_i	– molar weight of species i
W, M	– molar weight of mixture
σ_{ij}^2	– characteristic cross-section of i-j pair collision, Å^2

$\Omega_{ij}^{(1.1)}(T^*)$ – *i-j* collision-integral of (1.1) order (viscous type)

T^* –characteristic temperature in the Lennard-Jones inter-molecular interaction potential

$\Omega_{ij}^{(2.2)}(T^*)$ – collision-integral of diffusion-type

R^0 – universal gas constant

$R_i=R^0/W_i$ – gas constant of species *i*

c_{pi} – specific heat at constant pressure of *i*-th species

c_{vi} – specific heat at constant volume of *i*-th species

$R=\sum_{i=1}^{N} Y_i R_i$ – gas constant of mixture

$h=\sum_{i=1}^{N} Y_i h_i$ – specific enthalpy of mixture

$e=h-p/\rho$ – specific internal energy

β – Hall parameter, $\beta=\omega_e\tau_e$, ω_e is the gyro-frequency = eB/m_e, τ_e is the average time between impacts for electron

σ – electrical conductivity

$\mathbf{E}$ – electric field strength vector

$S_{x,y}$ – components of electromagnetic force [$\mathbf{j}\times\mathbf{B}$]

S_e – energy source due to work of electromagnetic force and radiation

Q_{rad} – radiation power

σ_{SB} – Stefan-Boltzman constant

$\nu'_{l,r}, \nu''_{l,r}$ – the stoichiometric coefficients of reagents and products, respectively

c_i – molar concentrations of species *i*, $c_i=\rho\cdot Y_i/W_i$

k_{fr} , k_{br} – forward and backward reaction rate constants

$\dot{w}_i$ – *i*-th species rate of mass due to chemical reactions

ω – computational domain volume

$\partial\omega$ – boundary of computational domain

$\mathbf{R}$ – residual-vector in the discrete Navier-Stokes equations

t^n – time value on *n*-th time-integration step

$\Delta t=t^{n+1}-t^n$ – time-integration step

$\mathbf{U}^n$, $\mathbf{U}^{n+1}$ – solution-vector at t^n and t^{n+1} time-level, respectively

$\mathbf{U}_i$ – intermediate solution-vectors in Runge-Kutta method

$\mathbf{U}_L$, $\mathbf{U}_R$ – left and right solution-vectors respective to integration-point (*ip*) position

$\psi_{P,E}$ – limiter-functions in linear-in-cell variable interpolation

I_{arc} – total arc current, discharge current

V_r – reacting volume measure

Q_i – total production of species i

Ω – integral vorticity of the flow